# Recent development of thermally assisted surface hardening techniques: a review Jun Liu<sup>1</sup>\*, Chang Ye<sup>2</sup>, Yalin Dong<sup>1</sup>

<sup>1</sup>Department of Mechanical Engineering, The University of Akron, Akron, OH 44325, USA

<sup>2</sup>State Key Laboratory of Digital Manufacturing Equipment and Technology, School of Mechanical Science and Engineering, Huazhong University of Science and Technology, Wuhan, Hubei 430074, China

\*Corresponding author e-mail address: J. Liu: <u>il200@zips.uakron.edu</u>

# **Table of Contents**

Abstract	2
1. Introduction	2
2. Warm shot peening	5
2.1. History, experimental setups, and materials	5
2.2. Roughness, mechanical characteristics, and mechanisms	6
2.2.1. Surface roughness	6
2.2.2. Hardness	7
2.2.3. Fatigue and residual stress	8
3. Warm laser shock peening	12
3.1. History, experimental setup, and materials	12
3.2. Roughness, mechanical characteristics, and mechanisms	13
3.2.1. Surface roughness	13
3.2.2. Hardness	13
3.2.3. Tensile properties	14
3.2.4. Fatigue	16
4. Thermally assisted ultrasonic surface hardening	18
4.1. History, experimental setup, and materials	18
4.2. Roughness, mechanical characteristics, and mechanisms	21
4.2.1. Surface roughness	21
4.2.2. Hardness	24
4.2.3. Friction and wear behaviors	26
5. Discussion	28
6. Conclusions and outlooks	31
6.1. Fatigue of thermally assisted ultrasonic surface hardening processed component	32

6.2. Corrosion.	32
6.3. Parameters optimization and computational methods	32
6.4. Application of thermally assisted surface hardening to ceramic and AM metals	s 32
6.5. Integration of thermally assisted surface hardening in additive manufacturing.	33
Nomenclature	34
References	35

#### **Abstract**

Thermally assisted surface hardening techniques have led to a surge in research efforts and industrial applications, with emphasis on strengthening of metallic materials with high work hardening, high strength and/or poor deformability. This paper reviews the development of common thermally assisted surface hardening techniques, including warm shot peening, warm laser shock peening, and thermally assisted ultrasonic surface hardening. The development and working principle for each of the techniques are discussed. The enhanced mechanical properties and corresponding mechanisms are reviewed in detail. As compared with conventional surface hardening techniques, thermally assisted surface hardening techniques with optimum processing temperatures can further increase the surface and subsurface hardness, thickness of the hardening layer, fatigue life, and wear resistance of mechanical components. The improvements are attributed to the unique microstructures fabricated by the synergistic effects of thermal energy and high-strain-rate plastic deformation. Thermal energy can soften the materials, allowing plastic deformation to produce higher magnitude and deeper region of work hardening. More interestingly, the thermomechanical treatment can also induce dynamic strain aging and dynamic precipitation in metallic alloys, which leads to precipitation strengthening and enhanced stability of dislocations and compressive residual stress. The coupled thermal-dynamic effect enables a broader design space for alloy hardening. Lastly, future research directions of thermally assisted surface hardening techniques are discussed.

*Keywords*: warm shot peening; warm laser shock peening; ultrasonic surface rolling processing; ultrasonic nanocrystal surface modification; thermally assisted surface hardening.

#### 1. Introduction

Surface hardening techniques such as shot peening (SP) [1], surface mechanical attrition treatment (SMAT) [2], laser shock peening (LSP) [3][4], and ultrasonic surface hardening [5][6], have been routinely employed to improve mechanical properties of components, including surface hardness, fatigue life, and wear resistance. Such improvements are realized through high-strain-rate plastic deformation induced by intensive impacts applied to the surfaces, which produce high-density dislocations, twins, and/or refined grains as well as compressive residual stress (CRS) in the surface and subsurface regions. Fig. 1 presents the schematics of common surface hardening techniques. SP and SMAT employ balls that made of metal, glass, or ceramic to bombard a component, dimpling the surface and causing local plastic deformation and shock waves in the material as shown in Fig. 1a. LSP adopts high-energy-density, short-duration laser pulses to produce rapid expanding plasma via ablation of a sacrificial layer on the surface of the component. The expanding plasma confined between the surface and a transparent confinement

layer produces shock wave, inducing plastic deformation in metal as shown in Fig. 1b. Ultrasonic surface hardening utilizes an electro-mechanical ultrasonic transducer to generate ultrasonic vibrations, driving a needle with a fixed tip or a rolling ball to impact the surface at ultrasonic frequency as shown in Fig. 1c. The devices based on this working principle, include ultrasonic impact treatment (UIT), ultrasonic surface rolling processing (USRP), and ultrasonic nanocrystal surface modification (UNSM).

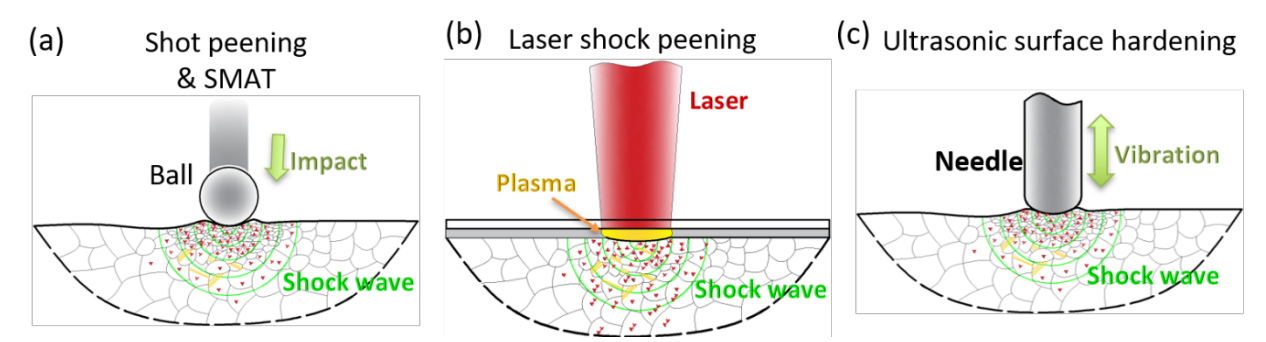


Fig. 1. Schematics of three types of surface hardening techniques: (a) SP and SMAT; (b) LSP; (c) ultrasonic surface hardening.

On the forefront of innovation in the automotive and aerospace industries, the demand for ultrahigh-strength materials has never ceased. The further increase of mechanical strength of materials without adding weight can push the limit for fuel efficiency, quality, and durability. However, it is challenging to effectively strengthen the materials with high strength, high workhardening, and/or low ductility for two reasons. Firstly, to further hardening high-strength materials, it requires more aggressive processing conditions such as longer processing time and higher pressure, which approach the limits of conventional surface hardening methods. Secondly, such aggressive processing conditions increase the likelihood of poor surface integrity and subsurface cracks for high strength materials often have relatively poor ductility. For examples, Liu et al. reported that internal cracks were produced in LSP processed 7050-T7451 aluminum alloy when the laser power density exceeded 3 GW/cm<sup>2</sup>, which reduced the fatigue life of the processed workpiece [7]. Unal and Varol investigated effects of SP Almen intensity on microstructure and mechanical properties of AISI 1017 mild steel [8]. It was found that high Almen intensity induced excessive plastic deformation, leading to surface cracks. Liu et al. reported that the large surface plastic deformation induced by UIT resulted in "folded defects" below the surface of the S69QL steel workpiece [9]. Feng et al. reported the presence of folded defects in the ultrasonic peening processed S355 steel [10]. Such defects are most probable fatigue crack initiation sites. Additionally, the high-strain-rate plastic deformation itself can decrease the efficiency of strengthening. For instance, processing of materials with high work hardening tendency, such as superalloys and stainless steels, the high-strain-rate plastic deformation can immediately produce a hardening layer in the top-most surface region with saturated dislocations, acting as an obstruction for the subsequent plastic deformation within the component. Furthermore, surface hardening processing of brittle materials such as ceramics, cemented carbides, and chrome plating, is regarded impossible since the materials could be damaged before plastic deformation occur. To address these challenges, thermally assisted surface hardening techniques have been developed, which involve simultaneous applications to a component of thermal energy and high-strain-rate plastic deformation. The thermal energy is applied to maintain a high working temperature of the component during processing, decreasing

the flow stress and brittleness temporarily, which allows the working tool to modify the microstructure more effectively.

In addition to improve the processing efficiency, thermal assisted surface hardening creates a new design space for microstructure modification due to its unique thermal-mechanical coupling effect. Mechanical properties are primarily determined by microstructures which largely depend on processing conditions, including strain, strain rate, and temperature. The addition of temperature creates a new dimension in the microstructure diagram, in which microstructure depends on strain, strain rate and temperature. Previous research activities on thermomechanical treatment (TMT) have demonstrated that the sum of plastic deformation and heat treatment is greater than the sum of the individual processes, resulting in either enhanced or completely new mechanical properties due to the unique microstructure resulted from the synergist effect of the treatments. Many metallic solid solutions undergo dynamic strain ageing (DSA) during plastic deformation at specific ranges of temperature [11]. The phenomenon originates from the interaction between moving dislocations and solutes, leading to instability in plastic flow of materials. Such phenomenon was interpreted using the concept of the Cottrell effect (or Cottrell atmosphere), which was firstly proposed by Cottrell and Bilby in 1949 [12]. For body-centered cubic (BCC) and face-centered cubic (FCC) interstitial alloys like steels, aluminum alloys, and nickel based superalloys, the small interstitial atoms, such as boron, carbon, or nitrogen can diffuse into the dislocation core and stay, hindering dislocation motion [13][14][15][16]. In addition to DSA, dynamic precipitation (DP) can take place during plastic deformation performed at certain temperatures. Dislocations produced by the plastic deformation act as favorable nucleation sites to facilitate the growth of precipitates. DP is more efficient in strengthening as compared with static ageing since DP occurs in a much shorter time. Therefore, the solute atoms and precipitated fine particles are sources of strengthening, which can improve the mechanical properties of TMT components as compared with conventional plastic deformation. For example, Kerscher et al. reported that TMT produced dissolved carbon atoms and small carbides in SAE52100 bearing steel via DSA, increasing the density and stability of the dislocation by pinning the dislocation motion, which prolonged the fatigue limit of the steels [17]. It is reported by Cai et al. that DSA and DP using equal channel angular extrusion performed at 170 °C increased the ultimate tensile strength (UTS) of the 6061 and 6069 aluminum alloys as compared to conventional static aging at the same processing temperature [18]. It is anticipated that thermally assisted surface hardening, as a TMT technique, would be able to tailor microstructure through thermal-mechanical synergistic mechanisms, leading to a new design space for material processing.

A typical thermally assisted surface hardening device is composed of two parts: a conventional surface hardening system and a heat source. The heat sources vary from primitive to technologically advanced, including oven [19], hot air [20], hot plate [21], electrical current [22], halogen lamp [23], and laser beam [24]. The technique has evolved persistently over the past two decades with the emergence of new surface hardening techniques, heat sources, and the pressing demand for processing materials with high mechanical strength. However, after years research, most valuable findings in this field are still limited at the laboratory scale. To unleash its potential and scale it up at the industry scale, the advantages and applicability of these techniques must be clearly demonstrated and documented. Towards this end, this work gives a comprehensive review of the history, as well as the latest advances of thermally assisted surface

hardening techniques, their effects on mechanical property improvement and corresponding mechanisms.

The paper will focus on surface hardening techniques that can realize high-strain-rate (>10<sup>3</sup> s<sup>-1</sup>) surface plastic deformation, including LSP, SP, USRP, and UNSM. According to the employed surface hardening technique, thermally assisted surface hardening techniques are categorized into three classes: warm shot peening (WSP), warm laser shock peening (WLSP), and thermally assisted ultrasonic surface hardening. WSP and WLSP will be reviewed in Section 2 and Section 3, respectively. Thermally assisted ultrasonic surface hardening, including thermally assisted USRP and UNSM, will be reviewed in Section 4. Each section includes an overview of the development history, experimental setup, processed materials, and the effectiveness of the technique on mechanical properties. Section 5 discusses the mechanisms of the different techniques in improving the mechanical properties of mechanical components. Lastly, the outlook of the current challenges and future directions of the techniques are presented. Summary tables of timeline, heat source, and modified mechanical properties, grouped by the surface hardening techniques are listed in Tables 1~3.

## 2. Warm shot peening

WSP is one of the very early attempts of thermally assisted surface hardening. The working principle of WSP is to heat up the target component to an elevated temperature, softening the material temporarily, and simultaneously process the component surface using conventional SP. This hybrid processing has been broadly employed to process mechanical components made of carbon steels, metal matrix composites, magnesium alloys, titanium and its alloys.

# 2.1. History, experimental setups, and materials

In 1989, NHK Spring Co., Ltd applied WSP to process automotive suspension coil springs with high design stress. In 1999, Tange et al. investigated effects of WSP on SUP7M spring steels [19]. To realize elevated working temperatures, coil springs were placed in a heat circulated oven, then were heated to certain temperatures. Another one of the very early study of WSP was carried out by the researchers from Germany in 1999 and 2000 [20][25]. A special nozzle was designed to realize SP at elevated temperature as shown in the illustration of Fig. 2 [26]. The workpiece was heated up by a second hot air flow which can maintain the workpiece temperature in the range of room temperature (RT) to 410 °C. Meanwhile, peening balls were accelerated by the primary cool air flow and then were employed to shot peen the workpiece.

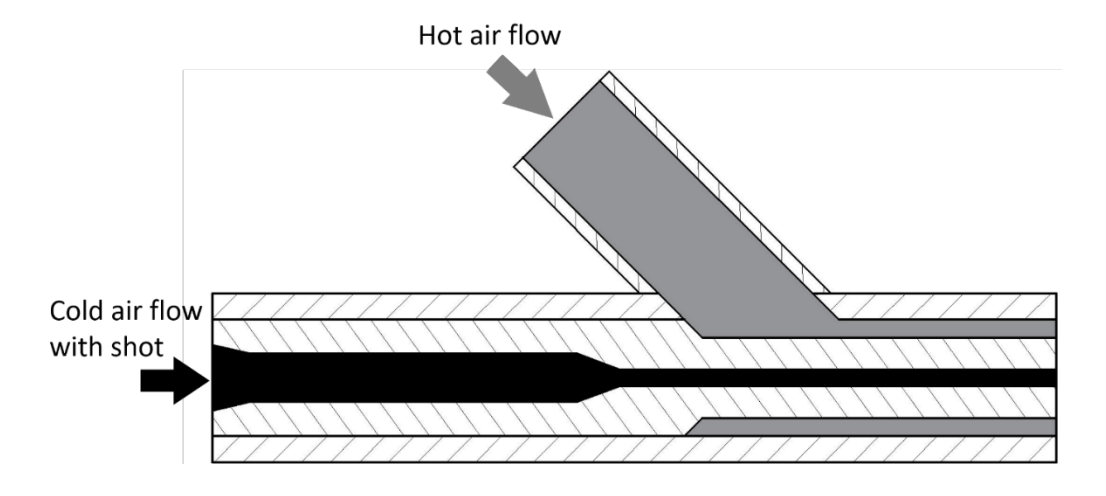


Fig. 2. Schematic of the nozzle designed for the WSP equipment used in [26]. (Reproduced with permission.)

Thereafter, researcher employed WSP to process TiB<sub>2</sub>/6351Al composite [27][28], commercially pure titanium and its alloy [29], and SiCw/6061Al composite [30][31]. In these studies, the workpieces were preheated to the target temperatures and held at the temperatures for a certain time in furnaces. Then the workpieces were taken out from the furnaces and then processed using conventional SP at RT. Note that the actual peening temperatures were lower than the preheating temperatures to some degree.

In 2014, Huang et al. studied effects of WSP on Mg-9Gd-2Y alloy [32]. In the study, a warm air blast machine was developed as shown in Fig. 3. Hot ZrO<sub>2</sub>-SiO<sub>2</sub> ceramic beads with a diameter of 0.45 mm were mixed with the hot air and were accelerated to shot peen the workpiece. A cold air flow was applied to maintain the working temperature at 240 °C during the WSP process.

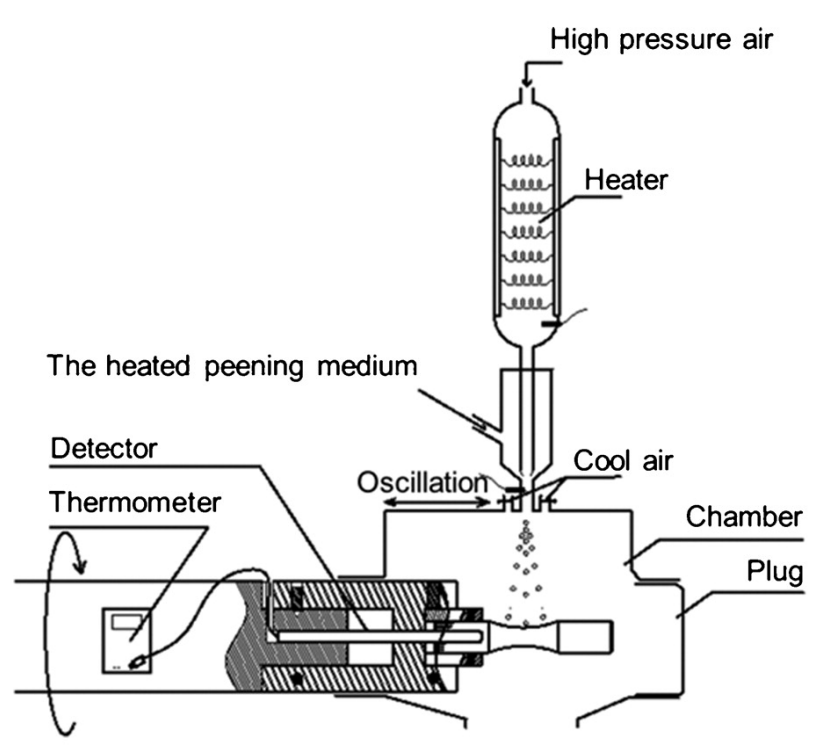


Fig. 3. Schematic of the warm air blast machine used in [32]. (Used with permission.)

# 2.2. Roughness, mechanical characteristics, and mechanisms

### 2.2.1. Surface roughness

As compared with conventional SP, WSP increases the surface roughness of components. Tange et al. reported that for SP of SUP7M spring steel, the maximum surface roughness increased from 10 μm to 14 μm with the working temperature increasing from RT to 350 °C [19]. For SUP9 spring steel, the surface roughness also slightly increased with the peening temperature increasing from RT to 500 °C as shown in Fig. 4a [33]. Wick et al. reported that the surface roughness of the AISI 4140 steel workpiece was increased from 8.1 μm to 11.3 μm by increasing the peening temperature from RT to 290 °C [20]. For Mg-9Gd-2Y alloy, the surface arithmetical mean roughness (Ra) of the WSP processed workpiece was consistently higher than that of the conventional SP processed one with the same peening intensity as shown in Fig. 4b [32]. The

surface roughness increment was attributed to the increased plastic deformation in the surface region caused by the elevated peening temperature [19].

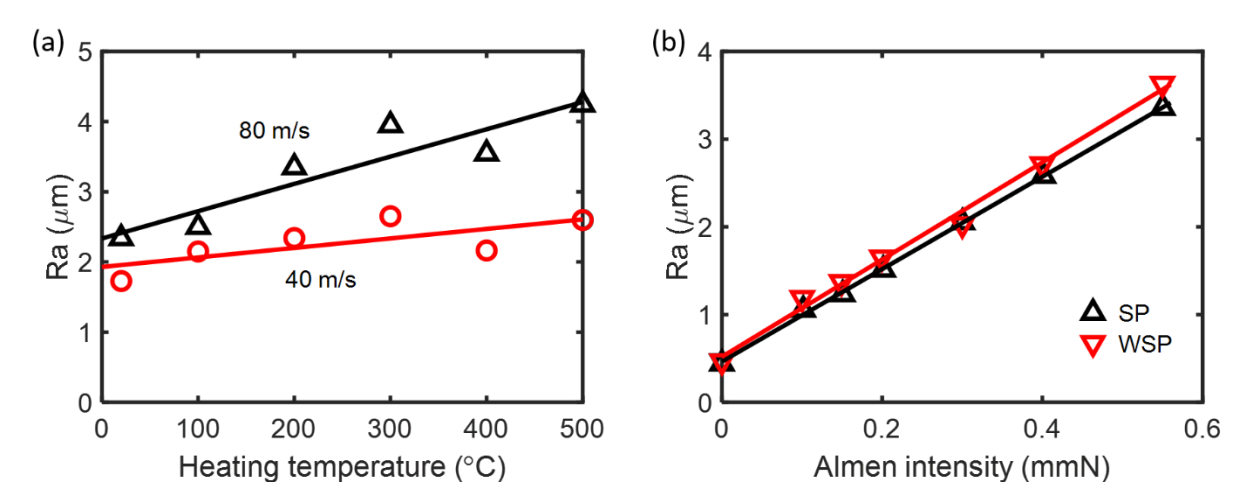


Fig. 4. (a) Relation between SP temperature and surface roughness of SUP9 spring steel [33]. (b) Relation between surface roughness and peening intensity of conventional SP and WSP processed Mg-9Gd-2Y alloy [32]. (Reproduced with permission.)

#### 2.2.2. Hardness

WSP can result in higher surface hardness and/or thicker hardening layer as compared with conventional SP [19][29][32][33][34]. For instance, Tange et al. measured hardness distributions of SUP7M spring steel after SP performed at RT, 100, 200, 300, and 350 °C [19]. It was found that, for the workpiece with initial hardness of 450HV, the SP performed at 350 °C can increase the surface hardness to a value that higher than 525HV. The hardness gradually decreased from the maximum value to the initial hardness with the distance from the surface, indicating a hardening layer was generated after WSP. On the contrary, the SP performed at RT did not show visible hardness increment in the surface region. Harada and Mori reported hardness distributions of SUP9 spring steel after SP performed at 20, 100, 200, 300, 400, and 500 °C as shown in Fig. 5 [33]. It is observed that, at elevated temperatures, SP can induce higher surface hardness and thicker hardening layer. Thomas and Jackson reported that, although WSP cannot notably increase the surface hardness of pure Ti as compared with conventional SP, but it can increase the hardening layer thickness approximately from 100 μm to 160 μm with the peening temperature increasing from RT to 280 °C [29].

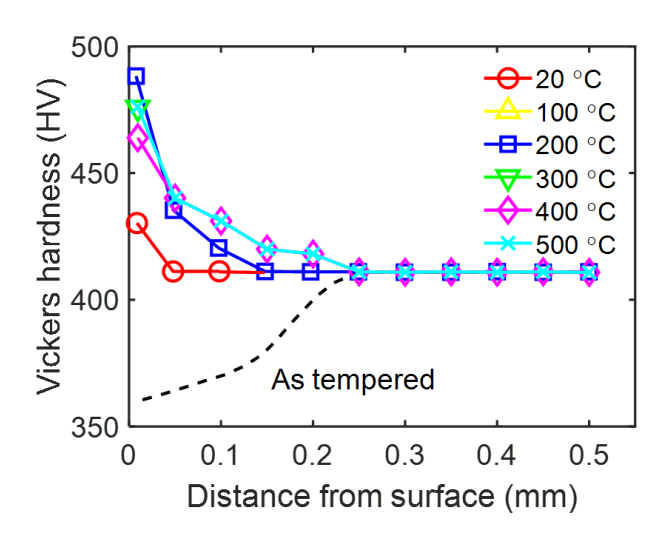


Fig. 5 Hardness distributions of SUP9 spring steel after SP performed at various temperatures [33]. (Reproduced with permission.)

Two mechanisms were proposed to explain the increased hardness induced by WSP. Tange et al. attributed the increased hardness to the resistance to the dislocation motion induced by solute atoms. Such solute atoms are produced through dynamic strain aging (DSA) and Cottrell effect promoted by the elevated working temperature during processing [19]. The other mechanism is that due to the elevated working temperature, more plastic deformation can be introduced into the surface and subsurface regions. The thermal energy can temporally annihilate the dislocations produced by the high-strain-rate plastic deformation in the top surface region and thereby decreases the flow stress of the material. By doing so, more plastic deformation can be produced via subsequent impacts in the subsurface region. As a result, a thicker strengthening layer with higher hardness can be produced in the surface and subsurface regions via WSP [29][32][33]. One should also note that WSP performed at higher temperature can lead to the decrease of the hardness due to the excessive softening effect [33].

## 2.2.3. Fatigue and residual stress

The most important benefit of WSP is its effect on fatigue. Most of the WSP studies reported that WSP can increase the fatigue life/strength of workpieces as compared with conventional SP [19][26][31][32][35]. For example, Menig et al. reported that the fatigue strength of SP processed AISI 4140 steel can be increased from 530 MPa to 704 MPa with increasing of the working temperature from RT to 330 °C as shown in Fig. 6a [26]. Huang et al. reported that, for Mg-9Gd-2Y alloy, SP performed at RT can increase the fatigue limit of the as extruded workpiece from 125 to 175 MPa [32]. In comparison, WSP performed at 240 °C increased the fatigue strength to 185 MPa as shown in Fig. 6b.

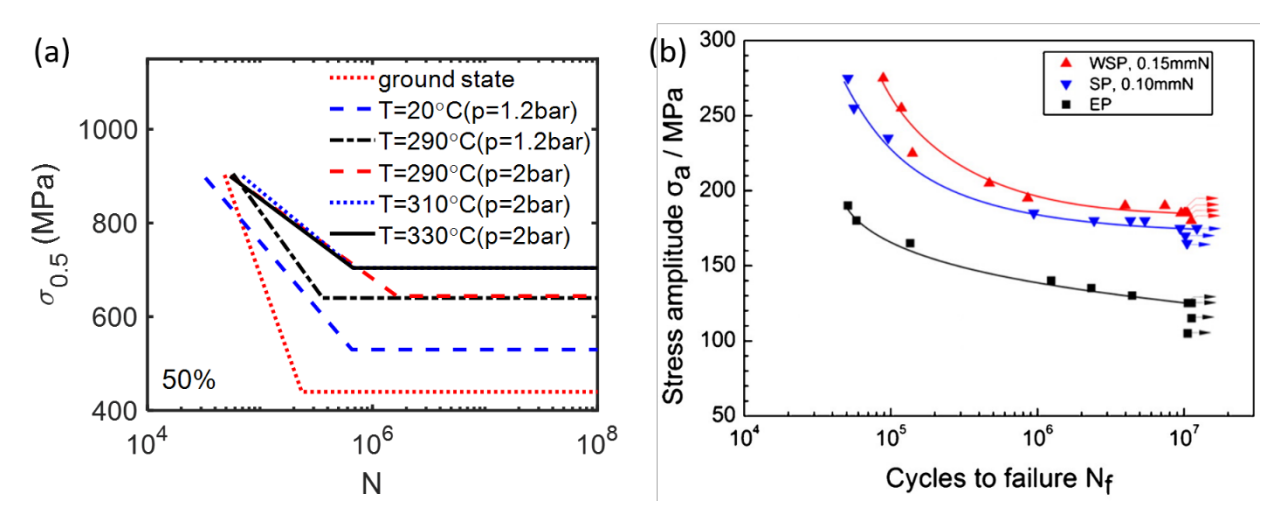


Fig. 6. S-N curves for SP and WLSP processed (a) AISI 4140 steel [26] and (b) Mg-9Gd-2Y alloy [32]. In Fig. 6a, *T* is the peening temperature and *p* is the hot air flow pressure as shown in Fig. 2. (Reproduced with permission.)

The extra fatigue life/strength caused by WSP was attributed to the higher magnitude of the CRS as compared with that of conventional SP. The residuals stress inside a component is in the equilibrium state, so the CRS on the surface produced by surface hardening results in the tensile residual stress inside the component. However, the initiation of fatigue cracks occurs on the surface due to cyclic loading stresses are maximum at the surface. The CRS in the surface region therefore can help to prevent the initiation of the cracks. Tange et al. found that CRS of spring steel workpieces processed using WSP at elevated temperatures were higher than that of conventional SP [19]. Luan et al. measured CRS of TiB<sub>2</sub>/Al composite after SP and WSP and found that WSP performed at 100 and 200 °C produced higher CRS in the subsurface region of the composite as shown in Fig. 7 [27]. The elevated working temperature leads to a decrease of flow stress and thus allows SP to produce more plastic deformation in the workpiece, producing a higher degree of CRS [32][33][34][36]. Therefore, the CRS can effectively arrest the crack propagation induced by the cyclic loading, increasing the fatigue life/strength of the workpiece.

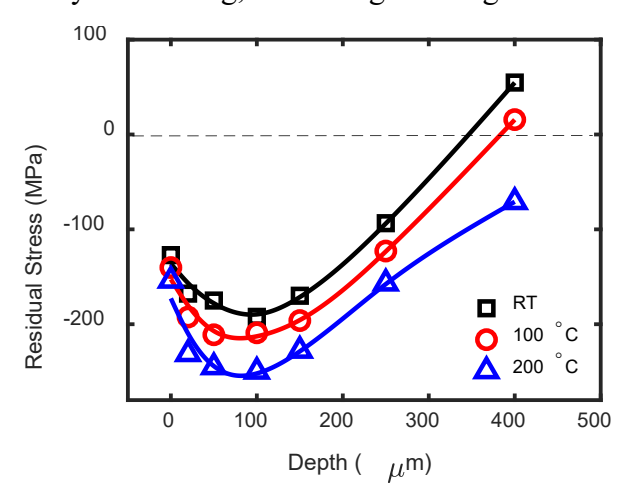


Fig. 7. Distributions of residual stress in thickness direction of TiB<sub>2</sub>/Al composite after SP performed at different temperatures [27]. (Reproduced with permission.)

The extra fatigue life/strength was also attributed to the increased stability of CRS, work hardening, and dislocation density [20][25][26][31]. Wick et al. employed X-ray technique to study stability of CRS and work hardening of AISI 4140 after SP and WSP process [25]. The residual stresses were determined using the sin<sup>2</sup> w method. The work hardening was evaluated using XRD line-profile analysis because the line broadening of Bragg diffraction peaks occurs due to dislocation multiplication and grain refinement. In order to characterize the stability, AISI 4140 workpieces after SP and WSP treatments were loaded with surface stresses for different numbers of cycles. Then RS and half width of the workpieces were measured. It was found that more RS were relaxed in conventional SP processed workpieces as compared with that of WSP workpieces as shown in Fig. 8a and 8b. For example, after 1000 cycles, the surface RS of the conventional SP workpiece decreased to 150 MPa, while that of the WSP workpiece was 380 MPa. Additionally, the authors also revealed that the WSP processed AISI 4140 had higher stability of work hardening and dislocation density as compared with the conventional SP processed workpiece as shown in Fig. 8c and 8d. It can be observed that after 1000 cycles, the surface half width of the conventional SP workpiece was reduced to 2.8°, whereas that of the WSP processed workpiece did not show visible change after the cyclic loadings. Huang et al. reported the same trend in SP and WSP processed SiC<sub>w</sub>/Al composites [31]. The higher stability was attributed to the DSA effect during WSP. As compared with SP performed at RT, the DSA effect was significantly enhanced by the elevated working temperature during WSP, which caused pinning of dislocations by solute carbon atoms and fine carbides in the steel [20][25][26] and by Mg<sub>2</sub>Al particles in the SiCw/Al composite [31], producing more diffusive and stable dislocation microstructures with beneficial CRS states.

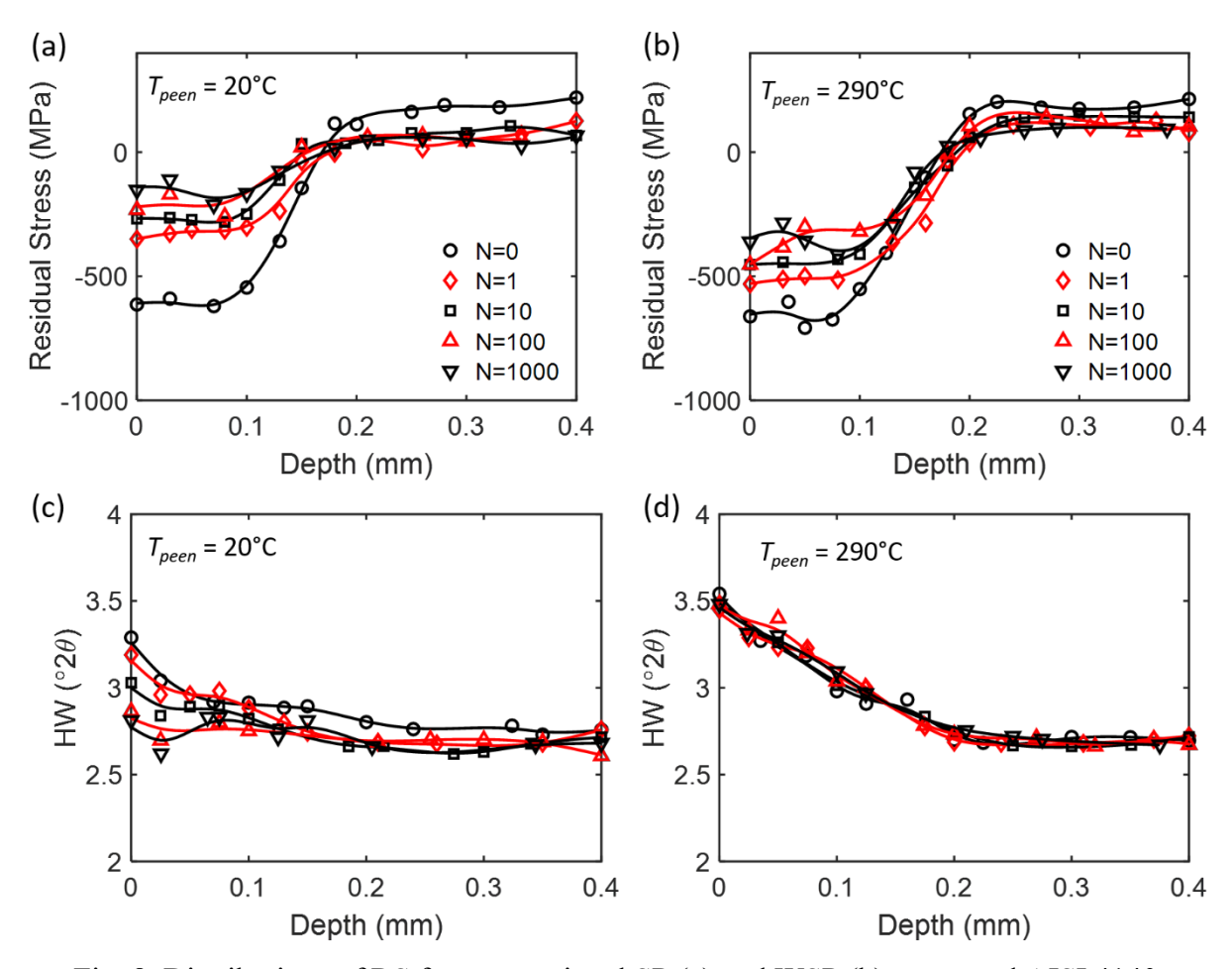


Fig. 8. Distributions of RS for conventional SP (a) and WSP (b) processed AISI 4140 workpieces; Distributions of half widths for conventional SP (c) and WSP (d) processed AISI 4140 workpieces [25]. (Reproduced with permission.)

Table 1. History, cited articles, processed materials, heat sources, working temperatures, and improved mechanical properties of WSP. The effectiveness is quantified by the mechanical property improvement (in %) resulted from the WSP performed at the optimal temperature in

comparison of the conventional SP. Improved mechanical Year Material Heat source Temperature properties SUP7M & RT, Heat 1999 [19] **UHS 1900** circulated 200~400 °C Fatigue & hardness (spring steels) oven 1999, 2000 **AISI 4140** Hot air flow RT, 290 °C Fatigue (20%) [20][25] Spring steel Heat 2002 [35] RT, 300 °C Fatigue (96.7%) & hardness SUP7 (SAE circulated 5160) oven 2002 [26] **AISI 4140** RT~410 °C Hot air flow Fatigue (21%) RT~450 °C, Spring steel 2005 [33] Plate heater Hardness (14%) SUP9 RT~500 °C

2007 [36]	carburizing steel SCM420, spring steel SUP9A	Furnace	RT~400 °C	NA
2008 [34]	Tool steel JIS- SKH51	Furnace	RT~300 °C	Hardening layer thickness
2008 [27]	TiB <sub>2</sub> /6351Al composite	Furnace	RT, <100 °C & < 200°C	NA
2009 [28]	TiB <sub>2</sub> /6351Al composite	Furnace	<100 °C and < 200 °C	NA
2012 [29]	CP-Ti, Ti-834	Chamber furnace	<280 ± 3 °C	Hardening layer thickness
2013 [30]	SiCw/6061Al composite	N/A	RT, <120 °C & < 170°C	N/A
2014 [32]	Mg-9Gd-2Y	Hot air flow and hot peening media	RT, 240 °C	Fatigue (6%) & hardness (8%)
2017 [31]	SiCw/6061A1	N/A	RT, <120 °C	Fatigue (18%)

# 3. Warm laser shock peening

WLSP was firstly developed by Ye et al in 2010 [37][38][39]. These early studies acknowledged the advantages of WLSP in fabricating unique microstructures and producing stable CRS via high-strain-rate plastic deformation, DSA, and dynamic precipitation (DP). It was evidenced that WLSP can improve the performance of a component subjected to cyclic loading at elevated testing temperatures. The technique has been widely applied to process aluminum alloys [37] [40], copper [38], carbon steels [21][40], and titanium alloys [41]. Research actives of WLSP from 2010 to 2016 were documented in the review paper of [42]. The present work will focus on research efforts reported thereafter.

# 3.1. History, experimental setup, and materials

In 2016, Prabhakaran and Kalainathan processed SAE 9254 (medium carbon low-alloy spring steel) using warm laser shock peening without coating (WLSPwC) [43]. The workpiece was preheated to 250 °C. During the processing, electrical dryers were employed to maintain the temperature workpiece. In the same year, Chen et al. reported WLSP processing of A356 aluminum alloy at temperatures of 25, 90, 120, 150, 180, and 210 °C [44].

From 2017 to 2019, WLSP was extensively applied to process Ti64 alloy [45][46], H62 brass [47], GH4169 superalloy (equivalent of IN718, UNS No. 7718) [48][49][50], and TC17 titanium alloy [51]. A schematic of WLSP is shown in Fig. 9 [48]. It consisted of a conventional LSP system and a heat source. The workpiece is placed on a heating table, which can maintain the elevated temperature during LSP. The confining layer can be a layer of glass [44][50] or silicone oil curtain with a vapor point of around 300 °C.

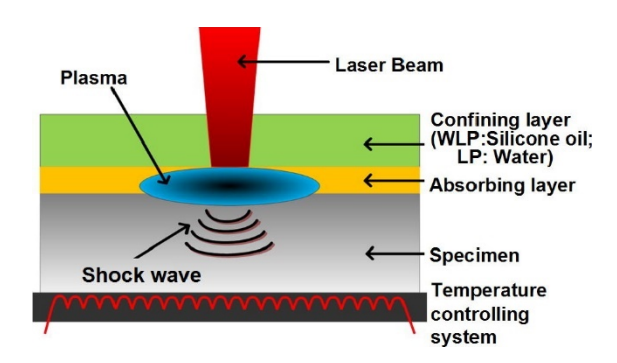


Fig. 9. Schematic of WLSP process [48]. (Used with permission.)

In 2019, Inamke et al. developed a dual-laser WLSP system as shown in Fig. 10 [52]. It consisted of a conventional LSP system and a continuous wave (CW) fiber laser system. The workpiece was placed in a silicon oil tank. The CW fiber laser beam was employed to heat the workpiece, which coincided with the laser spot of LSP to provide local heating. The technique was used to process laser-welded joints of AA6061-T6 and TZM alloys.

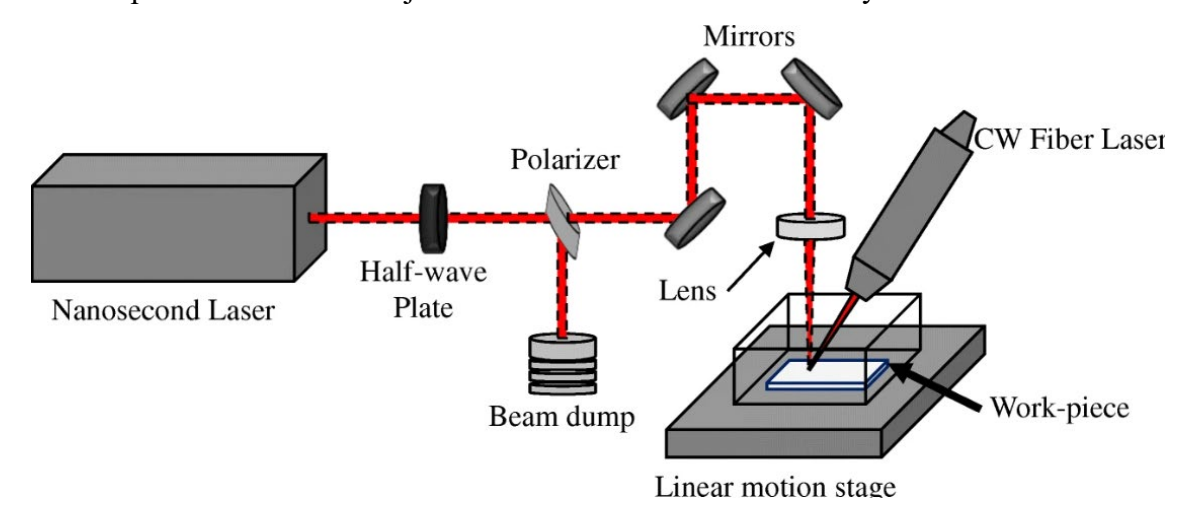


Fig. 10. Schematic of the WLSP system developed in [52]. (Used with permission.)

### 3.2. Roughness, mechanical characteristics, and mechanisms

#### 3.2.1. Surface roughness

Prabhakaran and Kalainathan reported the surface roughness of SAE 9254 workpieces processed using LSPwC and WLSPwC [43]. The average surface roughness was increased from  $1.13\sim1.51$   $\mu m$  to  $1.20\sim1.25$   $\mu m$  with the peening temperature increasing from RT to 250 °C. The increased surface roughness produced by WLSPwC was attributed to the thermal effect induced by the elevated peening temperature.

#### 3.2.2. Hardness

Many studies reported that WLSP can increase the surface and subsurface hardness as well as the hardening layer thickness in comparison of conventional LSP. For example, it was reported that WLSP increased the surface hardness of the SAE9254 steel workpiece to 11.34% from the LSP processed one as shown in Fig. 11a [43]. Hu et al. reported the hardness distributions of GH4169 superalloy workpieces processed by conventional LSP and WLSP as shown in Fig. 11b [49]. It was found that the maximum surface hardness of WLSP workpieces processed at 200, 250, and

300 °C registered 5.3%, 8.9%, and 13.0% growth as compared with that of the LSP workpiece. Chen et al. reported that, as compared with LSP, both surface hardness and hardening layer thickness of the WLSP processed A356 aluminum alloy were increased [44]. With the working temperature increasing from RT to 180 °C, the maximum hardness increased from 110.44 HV to 180.1 HV and the hardening layer thickness increased from 0.55 mm to 0.9 mm.

For the SAE9254 steel, the increased hardness was attributed to the higher dislocation density introduced by LSP performed at elevated temperature [43]. For the GH4169 superalloy, Hu claimed that, at elevated temperature, solute atoms can decrease the mobility of dislocations and thus increase dislocation multiplication, promoting grain refinement. That is to say, WLSP can further refine grains as compared with conventional LSP, which increased the surface hardness according to Hall–Petch strengthening [49]. Additionally, solute atoms produced via DSA further grow up to form nanoscale precipitates. These point defects are obstacles can anchor the dislocations and thus increase the material strength [44].

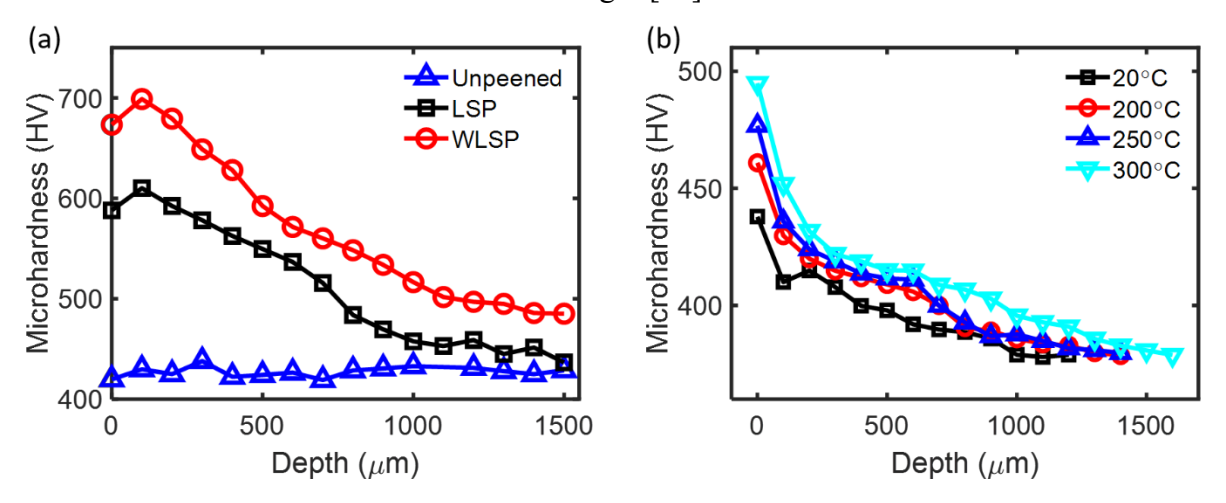


Fig. 11. Hardness distributions along the depth direction of LSP processed (a) SAE9254 steel [43] and (b) GH4169 superalloy [49] at various working temperatures. (Reproduced with permission.)

## 3.2.3. Tensile properties

Studies reported that as compared with conventional LSP, WLSP can result in better tensile properties such as yield strength (YS), ultimate tensile strength (UTS), and/or elongation [45][47][48][52]. For instance, Sheng et al. performed tensile tests on conventional LSP and WLSP processed IN718 superalloy [48]. The test results proved that WLSP can increase the strength and ductility of IN718 at RT and elevated temperature. As shown in Fig. 12a, when the tensile testing temperature was RT, the UTS of the workpiece increased from 528.78 MPa to 564.57 MPa and the YS increased from 282.87 MPa to 307.75 MPa with the peening temperature increasing from RT to 260 °C. Meanwhile, the elongation increased by 3.6%. Fig. 12b demonstrates that when the tensile testing temperature was 700 °C, the UTS increased from 491.64 MPa increased to 542.78 MPa the YS increased from 262.19 MPa to 289.50 MPa. The elongation increased by 10.6% with the peening temperature increasing. Meng et al. reported that the yield strength of the Ti64 workpiece increased from 983 MPa to 1075 MPa with the peening temperature increasing from RT to 300 °C as shown in Fig. 12c [45]. Lu et al. reported that the tensile strength of the H62 brass increased from 368 MPa to 389 MPa with the peening temperature increasing from RT to the DSA temperature as shown in Fig. 12d [47]. Meanwhile,

the strain up to plastic instability of the LSP workpiece demonstrated a 2.3% increase as compared with the as machined workpiece, while that of the WLSP workpiece was 27.4%.

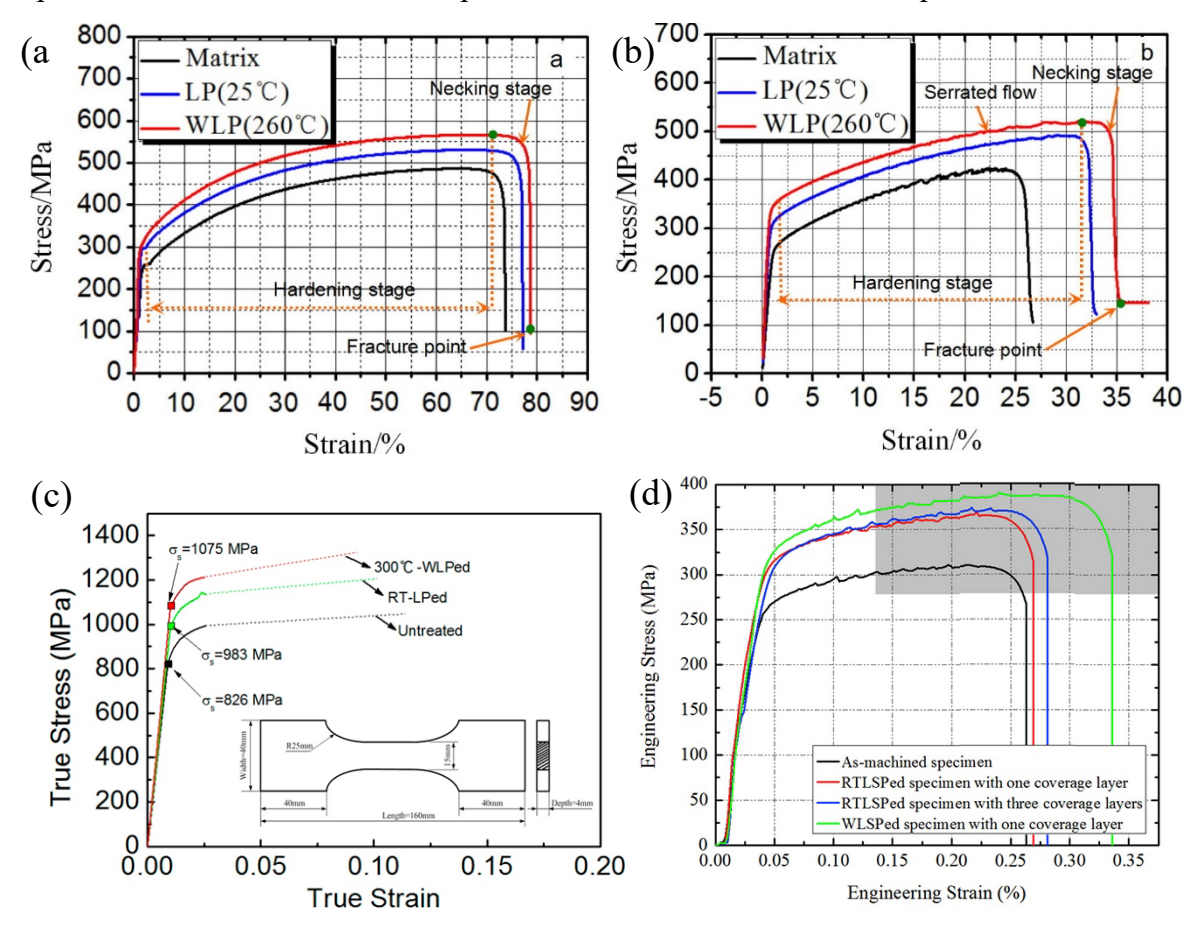


Fig. 12. Engineering stress-strain curves of the untreated (Matrix), LSP (LP), and WLSP (WLP) processed IN718 alloy (a) at RT and (b) 700 °C [48]. (c) True stress-strain curves of untreated, LSP, and WLSP processed Ti64 alloy [45]. (d) Engineering stress-strain curves of untreated (asmachined), LSP, and WLSP processed H62 brass [47]. (Used with permission.)

The strengthening mechanism was elucidated by the unique microstructure fabricated through WLSP. For the cases of IN718 superalloy and H62 brass, WLSP produced unique microstructures through plastic strain, DSA, and/or DP, including high densities of dislocation lines, dislocation tangles, dislocation arrays, mechanical twins, and/or precipitates [47][48]. For example, the microstructure of the WLSP processed IN718 superalloy is shown in Fig. 13. Such highly tangled structure was believed to be beneficial for the mechanical properties at both RT and elevated temperatures. For the case of Ti64 alloy, the extra strengthen resulted from WLSP was attributed to the increased plastic strain induced by laser peening at elevated temperature, which led to an increased dislocation density [45].

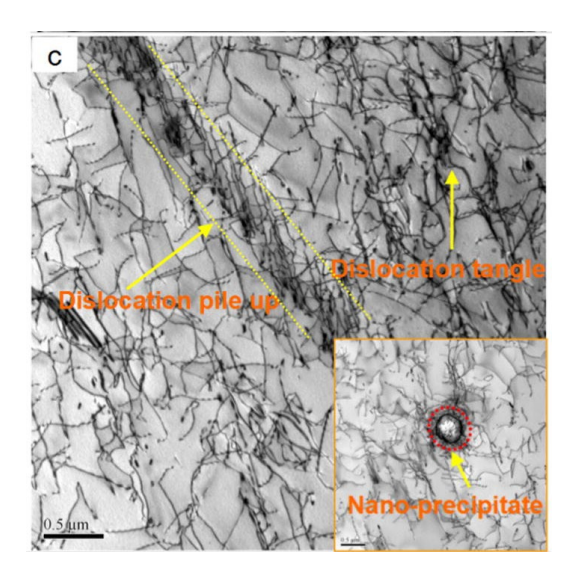


Fig. 13. TEM images of the microstructure of IN718 alloy after WLSP process [48]. (Used with permission.)

## 3.2.4. Fatigue

Studies reported that WLSP can result in higher fatigue life for metal components than conventional LSP. Prabhakaran and Kalainathan carried out tension-compression fatigue tests on LSPwC and WLSPwC processed SAE9254 spring steel [43]. It was found that the fatigue life was increased from  $10.95 \times 10^5 - 15.59 \times 10^5$  cycles to  $21.42 \times 10^5 - 28.84 \times 10^5$  cycles with temperature. Meng et al. conducted fatigue tests on LSP and WLSP processed Ti64 alloy [45]. Under 400 MPa, 765 MPa, and 850 MPa tensile stress, fatigue lives of the workpieces processed by LSP were  $8.8 \times 10^4$ ,  $2.2 \times 10^4$ , and  $0.5 \times 10^4$  cycles, whereas those of the WLSP workpieces were  $14.8 \times 10^4$ ,  $4.1 \times 10^4$ , and  $0.7 \times 10^4$  cycles, respectively.

It has been revealed that for FCC and BCC interstitial alloys, the elevated working temperature during WLSP can increase the DSA and DP effects, leading to formations of solute atoms and nanoscale precipitates, which can pin the dislocations produced by LSP. Such pinning effect significantly improve the RS stability and thus extend the fatigue life [42]. For Ti64 alloy, WLSP can improve the fatigue performance via increasing the damping ratios of the material [46]. Impact modal tests were carried out for LSP and WLSP processed Ti64 workpieces and it was found that the damping ratios increased with the increasing of the working temperature as shown in Fig. 14. Higher damping ratios can significantly decrease the vibration displacement and stress during fatigue tests, resulting in a lower fatigue crack growth rate. This increased damping ratios were attributed to the unique microstructure generated by WLSP as shown in Fig. 15. The microstructure of the Ti64 alloy workpiece was composed of β grains and schistose α grains inside the β grains as shown in Fig. 15a. The plastic deformation induced by LSP generated more schistose α grains inside the β grains, forming a basketweave structure as shown in Fig. 5b. After WLSP, the volume fraction of the interweaved acicular a grains increased significantly with the increasing of the working temperature as shown in Fig. 15c. This microstructure can significantly enhance the internal friction of the material and thus increase damping ratios.

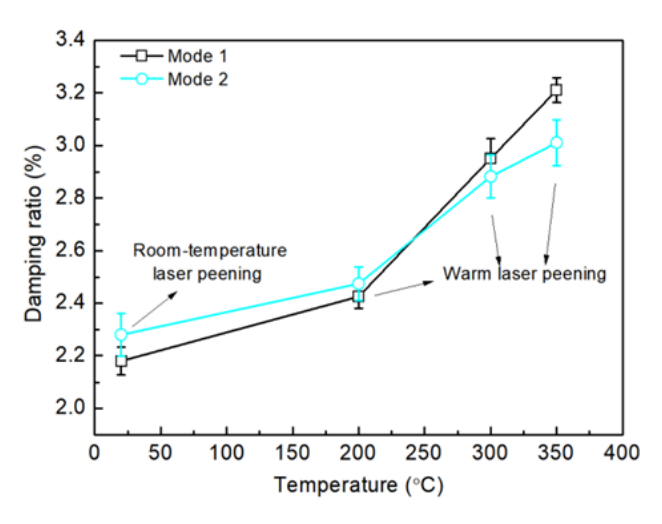


Fig. 14. Damping ratios as a function of LSP working temperature [46]. (Used with permission.)

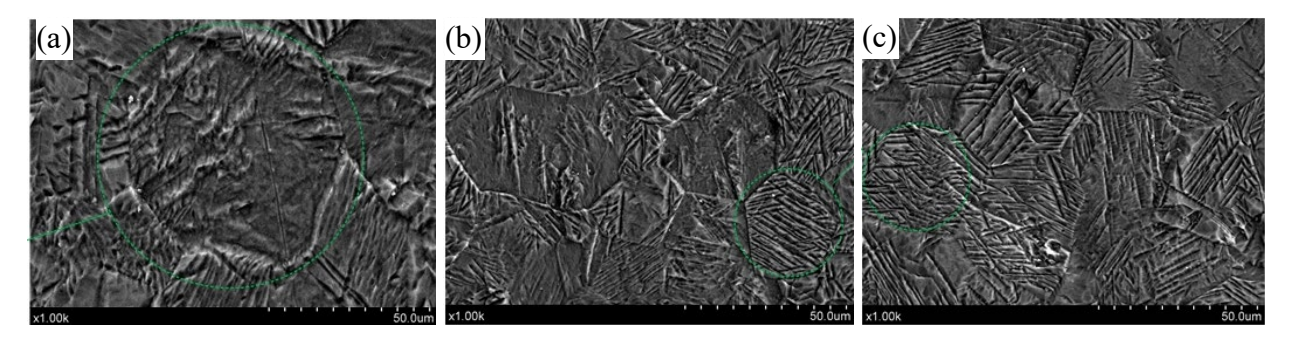


Fig. 15. Microstructures of the (a) untreated, (b) LSP, and (c) WLSP processed Ti64 workpieces [46]. (Used with permission)

Table 2. History, cited articles, processed materials, heat sources, working temperatures, and improved mechanical properties of WLSP. The effectiveness is quantified by the mechanical property improvement (in %) resulted from the WLSP performed at the optimal temperature in comparison of the conventional LSP.

Year	Material	Heat source	Temperature	Improved mechanical properties
2010 [37]	AA6160-T6	Hot plate	RT and 160 °C	Fatigue (7.5%) & hardness (36.8%)
2010 [39]	AA6160	Hot plate	RT, 80 and 160 °C	NA
2010 [38]	Cu	Hot plate	RT, 130, 230 °C	NA
2011 [21]	AISI 4140	Hot plate	RT~350 °C	Fatigue (6.7%) & hardness (7%)
2011 [40]	AISI1042	N/A	RT and 500 K	Hardness (7.7%)
2015 [41]	Ti64	Heating stage	RT~400 °C	Fatigue (48%)
2016 [43]	SAE9254	Electrical dryer	RT, 250 ± 15 °C	Fatigue (86.4%) & hardness (11.34%)
2016 [44]	A356 alloy	Heating table	RT~210 °C	Hardness (63.1%)

2017 [48]	IN718	Heating stage	RT, 260 °C	UTS (6.8% at RT, 10.4% at 700 °C), YS (8.8% at RT, 10.4% at 700 °C) & elongation (3.6% at RT, 12% at 700 °C)
2017 [45]	Ti64	Heating stage	Rt, 300 °C	YS (9.5%) & fatigue (49%~86%)
2017 [47]	H62 brass	N/A	DSA	UTS (5.7%) & ductility (24.5%)
2018 [49]	GH4169 superalloy	N/A	RT, 200~300 °C	Hardness (13%)
2019 [52]	AA6061-T6, TZM alloy	Fiber laser	425~500 K	AA6061 UTS (13.7%) elongation (14.0%), TZM elongation (13.0%)
2019 [46]	Ti64	N/A	200~350 °C	Fatigue (45.1%)
2019 [51]	TC17 titanium alloy	N/A	25, 100, 200, and 300 °C	N/A
2019 [50]	GH4169 superalloy	Heating pedestal	RT, 300 °C	N/A

## 4. Thermally assisted ultrasonic surface hardening

Ultrasonic surface hardening technique employs ultrasonic vibrations to drive a working tool, such as a fixed needle or a rolling ball, impacting the surface of a mechanical component at extremely high frequency [53]. USRP and UNSM are two common ultrasonic surface hardening techniques that have been integrated with various heat sources to realize thermally assisted surface hardening. The introduction of USRP and UNSM can be found in [54][55]. Since the working principles of USRP and UNSM are very similar, they will be reviewed together in this section.

## 4.1. History, experimental setup, and materials

In 2017, Gang et al. developed a thermally assisted USRP technique and the schematic of the equipment is shown in Fig. 16a [56]. The cylindrical workpiece was heated using a copper sleeve wrapped by a heating wire and be treated by a conventional USRP process at the same time. The technique was employed to process hot isostatic pressing (HIP) Ti64 alloy at working temperatures of 80, 120, and 160 °C. In the same year, Amanov et al. developed a high temperature (HT) UNSM process as shown in Fig. 16b [23][57]. A halogen lamp was employed to heat the workpiece and a fan served to cool down the system. A gold-coated reflector was designed to reduce the reflectance of the heat flux and concentrate the flux on the workpiece. The technique can realize very high working temperature that up to 1000 °C and it has been applied to process Ti64 alloy [23][57], tantalum (Ta) [58][59], IN690 [60], and stainless steel 316L produced by selective laser melting [61].

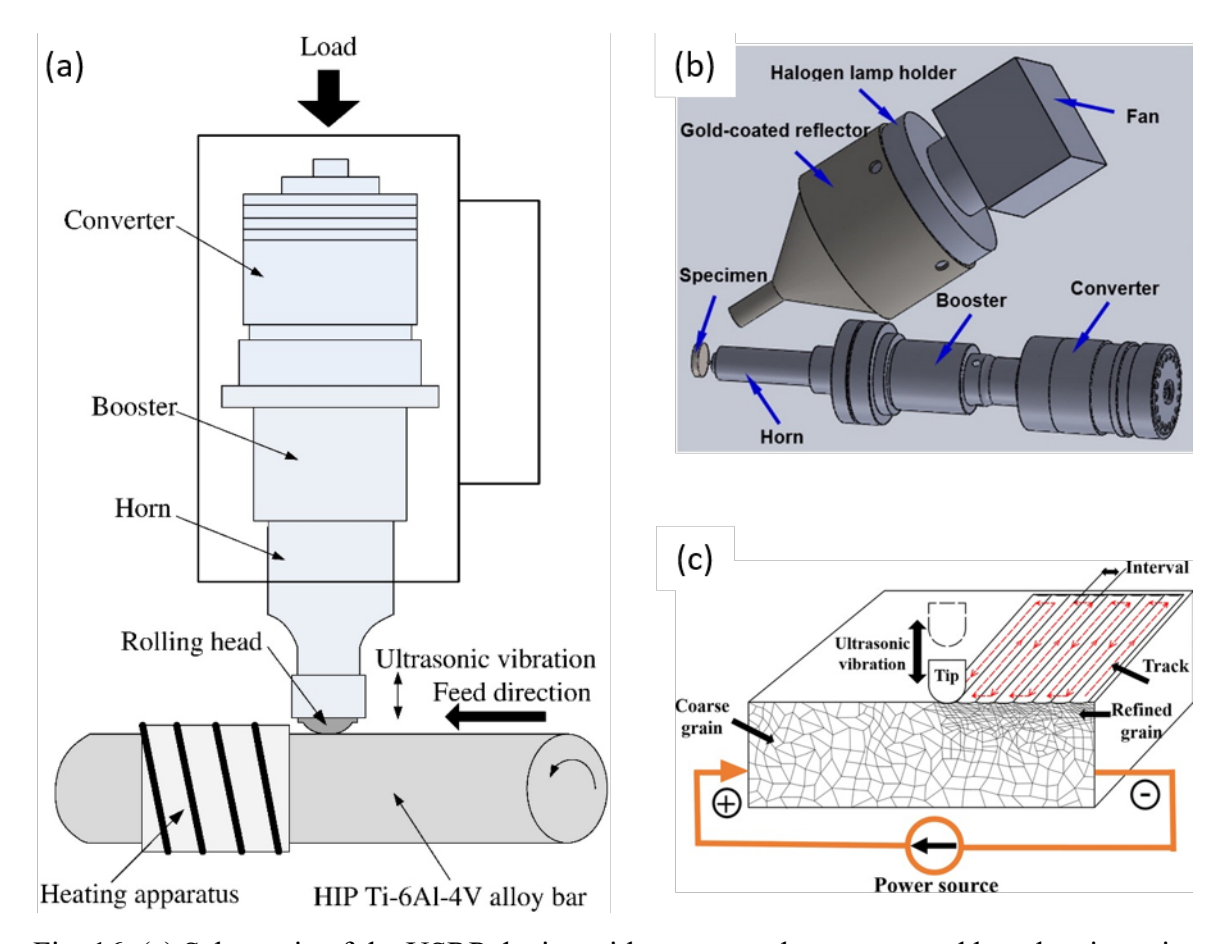


Fig. 16. (a) Schematic of the USRP device with a copper sleeve wrapped by a heating wire developed by [56], (b) the UNSM device with a halogen lamp heating apparatus developed in [23], and the EA-UNSM process developed in [22]. (Used with permission.)

In 2018, Jun et al. developed an electrically assisted UNSM (EA-UNSM) technique, which employed a direct continuous (DC) current as the heat source [22]. As shown in Fig. 16c, during an EA-UNSM processing, the workpiece was charged with DC current, inducing resistive heating, which can increase the temperature of the workpiece. The technique has been applied to process traditional casting and additive manufactured (AM) Ti64 alloys [22][62].

In 2019, Jun et al. developed a laser-assisted UNSM (LA-UNSM) technique to process Ti64 alloy [24]. LA-UNSM composed of an UNSM system and a CW fiber laser system as shown in Fig. 17a and 17b. The working principle of the LA-UNSM process is shown in Fig. 17c. During a LA-UNSM treatment, the workpiece can be locally heated by the laser beam and then immediately processed by the UNSM tool. The material at the tip-workpiece contact zone can be heated rapidly to a sufficiently high temperature. This localized heating approach is potentially adaptable because undesired heating of the subsurface can be avoided.

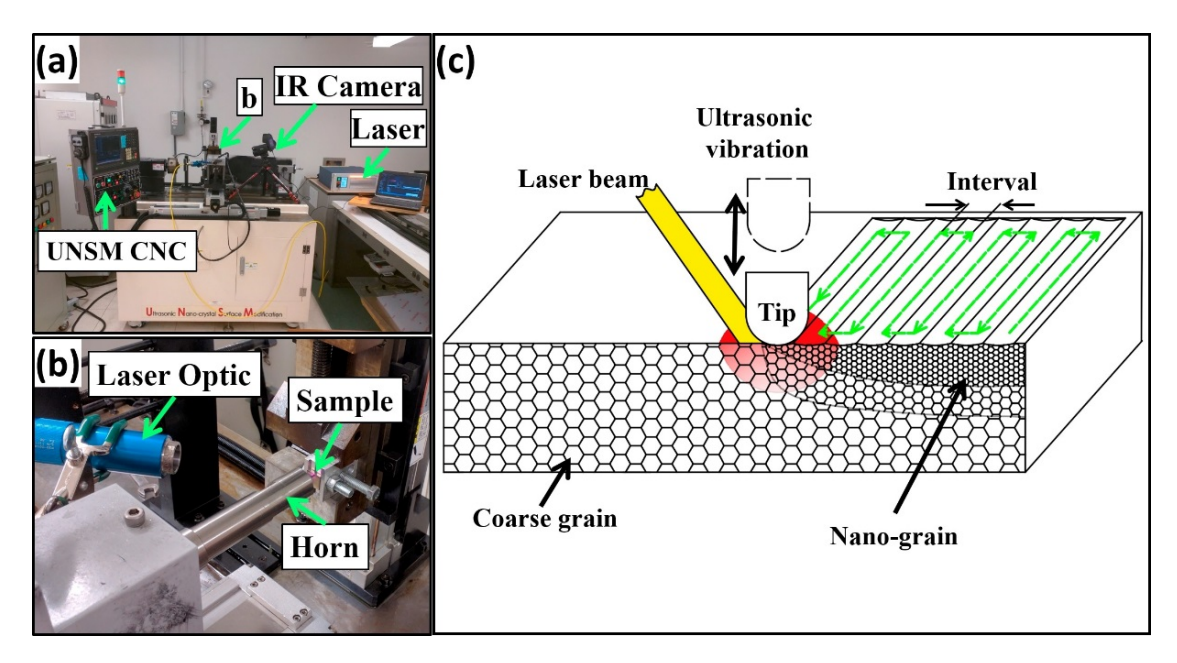


Fig. 17. LA-USNM system developed in [24]. (Used with permission.)

In 2020, Wang et al. developed an DC-USRP system, which combined a conventional USRP device with a DC power as shown in Fig. 18a [63]. The technique was applied to process AM Ti64 alloy. Luan et al. developed an ultrasonic hot rolling technique and used it to process 45CrNiMoVA ultra-high-strength steel [64]. The processing device is shown in Fig. 18b. Half of the steel cylinder surface was heated by an open furnace. An ultrasonic rolling tool was employed to process the surface of the workpiece. In the same year, Kim et al. studied effects of UNSM performed at RT and 300 °C on Fe-15Mn-1.2Al-0.6C high-Mn steel [65].

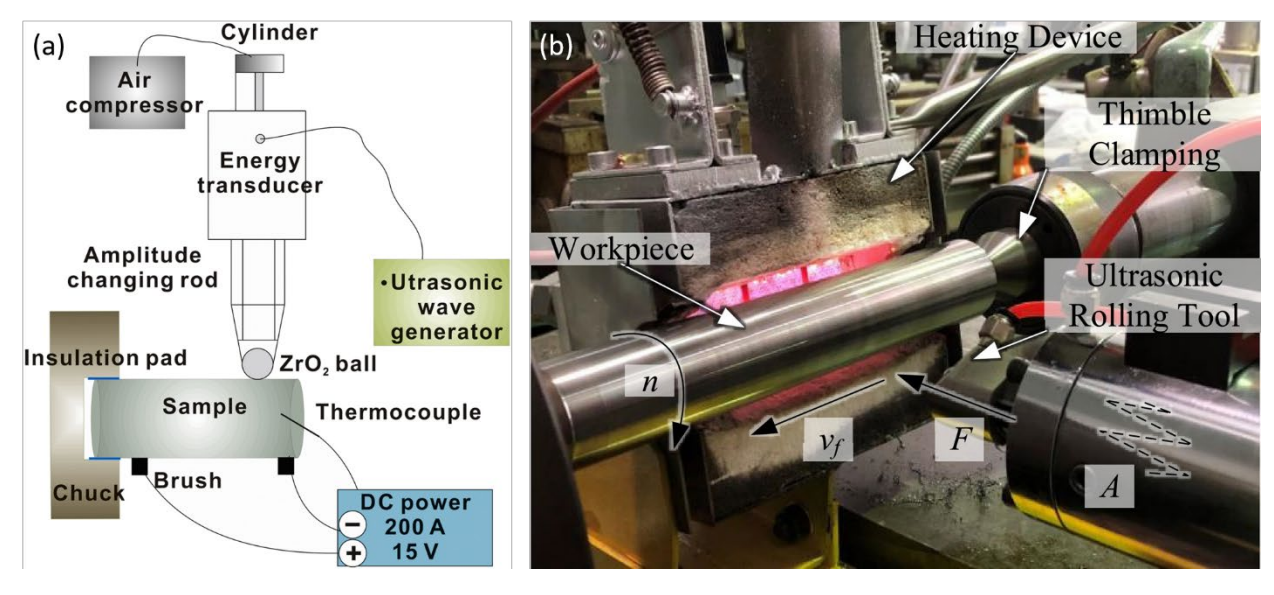


Fig. 18. (a) Schematic of the DC-USRP system [63] and (b) ultrasonic hot rolling device developed in [64]. (Used with permission.)

### 4.2. Roughness, mechanical characteristics, and mechanisms

# 4.2.1. Surface roughness

There is an inconsistency in the effect of thermally assisted ultrasonic surface hardening on the roughness. Some works reported that USRP or UNSM performed at elevated temperatures can increase the surface roughness as compared with its conventional counterpart [22][60]. For example, as shown in Fig. 19, Jun et al. demonstrated that Ra and the root mean squared roughness (RMS) of the UNSM processed Ti64 workpieces were increased from 0.266 µm and 0.353 µm to 0.376 µm and 0.468 µm with the working temperature increasing from RT to 320+ °C [22]. However, other researchers reported that with the increasing of the working temperature, the surface roughness of the processed workpiece can be reduced [23][62][63]. For instance, Amanov et al. reported that with the working temperature increasing from 400 °C to 800 °C, the surface roughness Ra of the UNSM processed Ti64 workpiece was gradually decreased as shown in Fig. 20 [23]. This inconsistency could be resulted from the different working temperatures and/or the different processing parameters in addition to original surface roughness of the target metals.

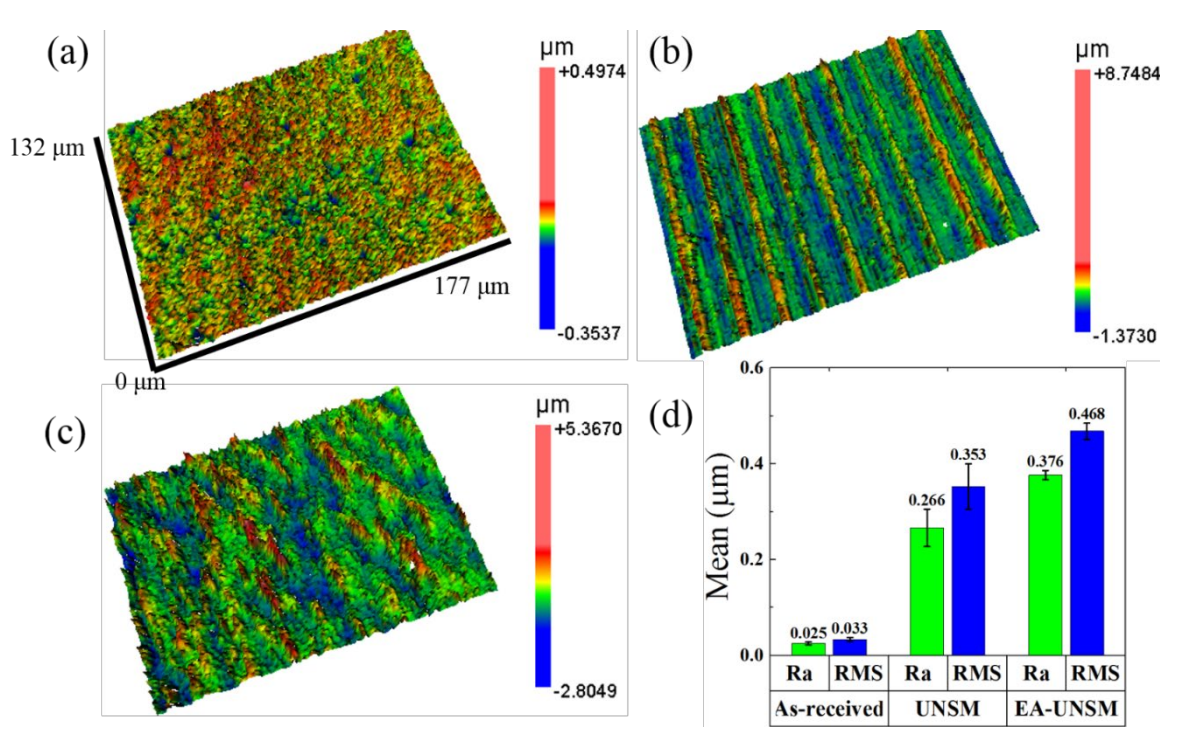


Fig. 19. Topography of as-received (a), UNSM (b), and EA-UNSM (c) processed Ti64 alloy. (d) Root mean squared roughness (RMS) and Ra of the Ti64 workpieces in different status [22]. (Used with permission.)

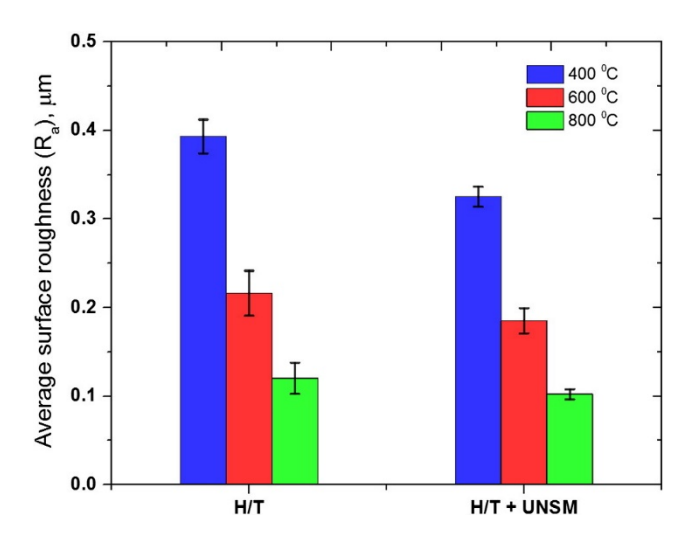


Fig. 20. Surface roughness Ra of the heat treated only (H/T) and thermally assisted UNSM (H/T+UNSM) processed Ti64 workpieces [23]. (Used with permission.)

However, higher process temperature usually leads to future reduction of the roughness of AM metals after thermally assisted USRP and UNSM. For example, it has been reported that the surface roughness Ra of the as-AM Ti64 workpiece was reduced to 7.1 μm after the conventional UNSM treatment, while that of the EA-UNSM processed workpiece was decreased to 1.3 μm [62]. Surface profiles and corresponding SEM images of the as-AM, UNSM, and EA-UNSM processed workpieces are shown in Fig. 21. It can be observed that the workpiece processed using EA-USNM has the smoothest surface and lowest pore density. In a more recent study, Wang et al. confirmed that the surface roughness Ra of the AM Ti64 workpiece can be reduced from 0.25 μm to 0.18 μm after USRP with the working temperature increasing from RT to 300 °C as shown in Fig. 22 [63]. This is because the as-AM surface usually has poor surface finish with porous structure and semi-melted powder particles. The elevated working temperature can soften the material and make the surface easier to deform. Therefore, the thermally assisted UNSM and USRP can reduce the surface roughness of AM materials more efficiently than their conventional counterparts.

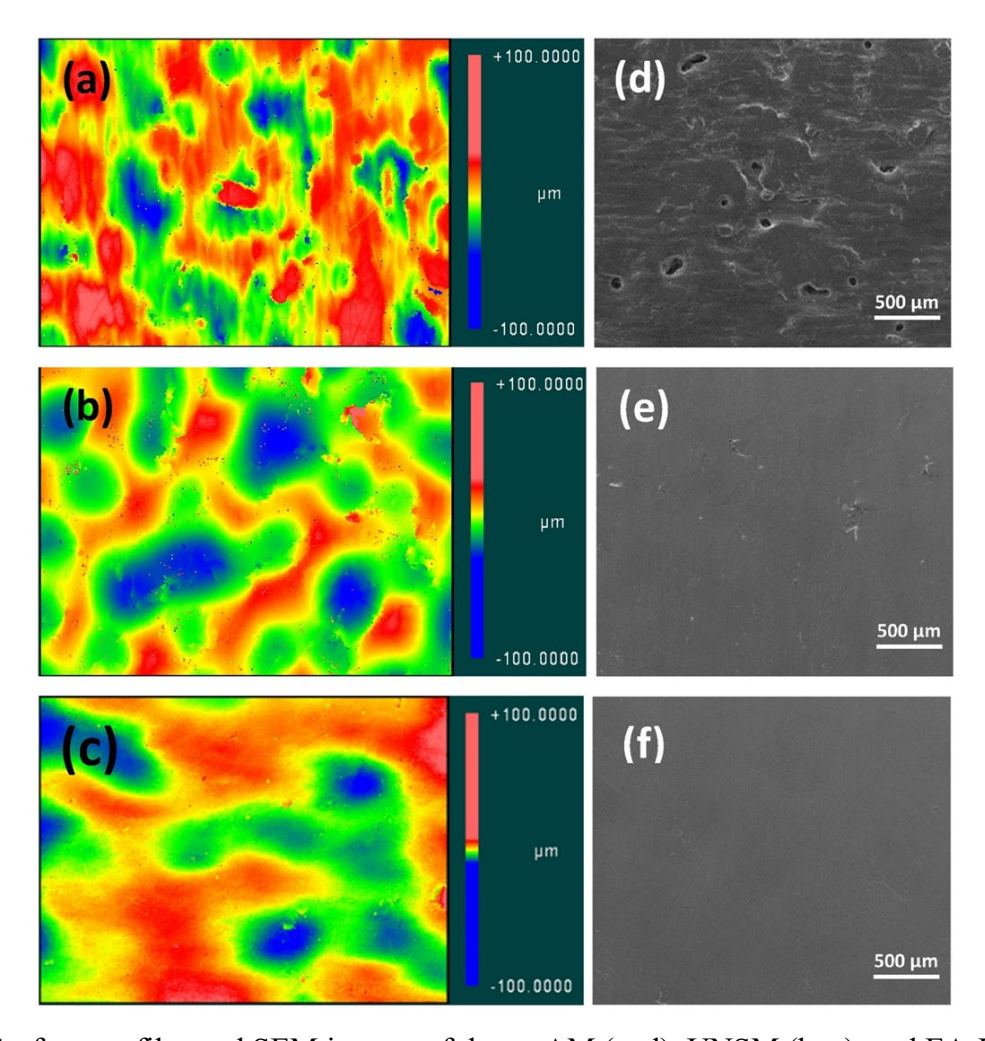


Fig. 21. Surface profiles and SEM images of the as-AM (a, d), UNSM (b, e), and EA-UNSM (c, f) processed workpieces [62]. (Used with permission.)

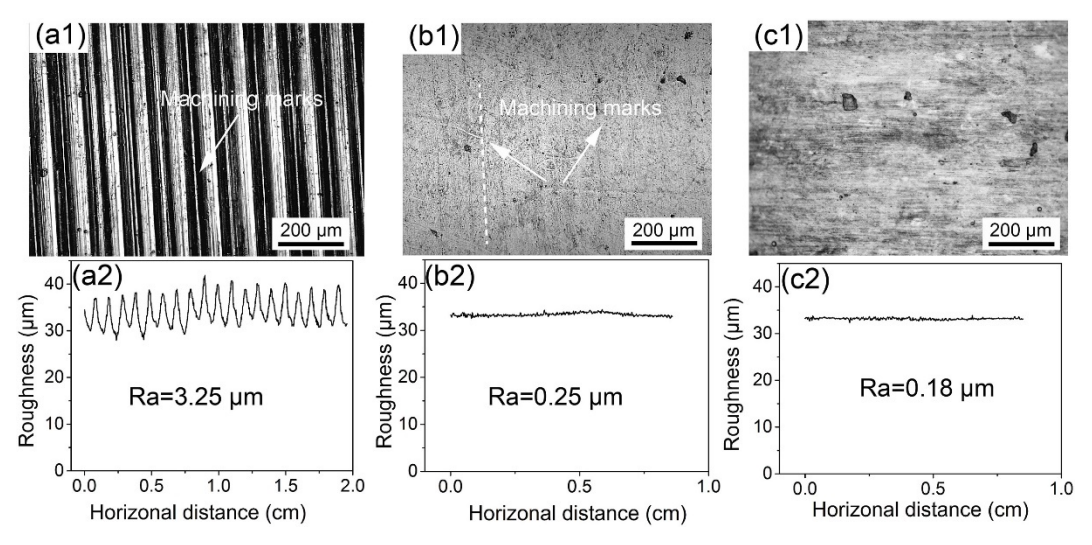


Fig. 22 Surface morphology and roughness of the as-machined (a), USRP (b), and DC-USRP processed Ti64 workpieces [63]. (Used with permission.)

#### 4.2.2. Hardness

Most of previous works reported that within specific range of temperature, thermally assisted UNSM and USRP can increase the surface hardness and/or hardening layer thickness as compared with their conventional counterparts [22][23][24][57][58][62][63]. For example, as shown in Fig. 23a, after processing of Ti64 workpieces, it was found that the EA-UNSM performed at 320+ °C can notably increase the subsurface hardness and hardening layer thickness as compared with the conventional UNSM [22]. The surface hardness of the AM Ti64 workpieces was increased from 3.90 GPa to 4.25 GPa with the working temperature increasing from RT to 300 °C as shown in Fig. 23b [63]. Higher surface hardness and thicker hardening layer have also been reported after UNSM processing at 300 °C for Ti64 alloy [60]. Further increasing the working temperature to 700 °C resulted in a decrease of the surface hardness due to the excessive softening effect. Li et al. showed that, for Ti64 alloy, USRP performed at 80, 120, and 160 °C resulted in a lower surface hardness as compared with conventional USRP. As shown in Fig. 24 [56], the highest surface hardness of the thermally assisted USRP workpieces was 414 HV, which was processed at 120 °C, while the highest surface hardness of the conventional USRP processed workpiece was 425 HV.

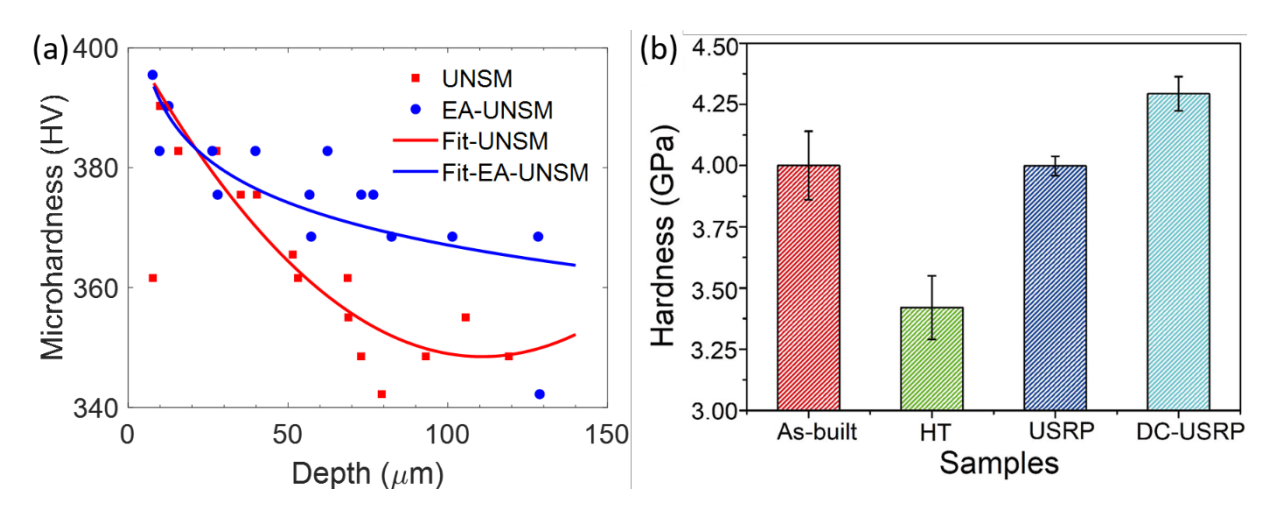


Fig. 23. (a) In-depth hardness distributions of the Ti64 UNSM and EA-UNSM processed workpieces [22]; (b) surface hardness of AM Ti64 workpieces after different processes [63]. (Used with permission.)

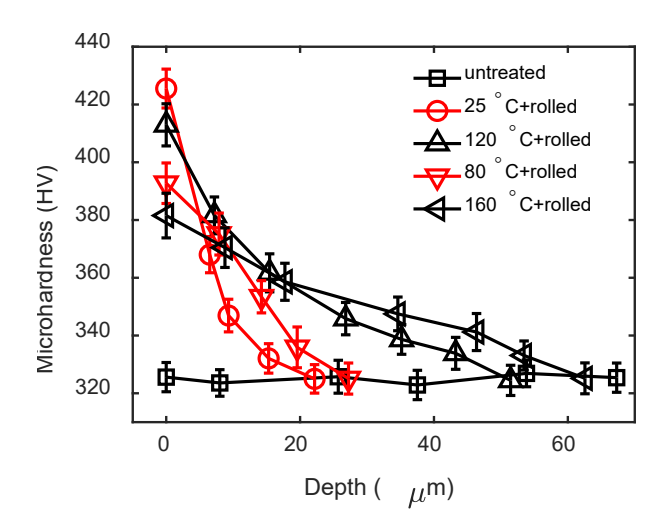


Fig.24 In-depth hardness distributions of the untreated, and USRP treated Ti64 workpieces at RT, 80, 120, and 160 °C [56]. (Reproduced with permission)

The increase in the thickness of the hardening layer was attributed the softening effect induced by the elevated working temperature, which can decrease the flow stress of the material and allow the working tool to induce more plastic deformation in the surface and subsurface regions. For example, it was reported that the severe plastic deformation (SPD) layer of the LA-UNSM processed Ti64 workpiece was about 50  $\mu$ m, while that of the conventional UNSM processed one was about 20  $\mu$ m as shown in Fig. 25 [24]. Wang et al. reported that, for the AM Ti64 alloy, the thickness of the heavily deformed layer increased from 180  $\mu$ m to 250  $\mu$ m after USRP with the working temperature increasing from RT to 300 °C as shown in Fig. 26 [63].

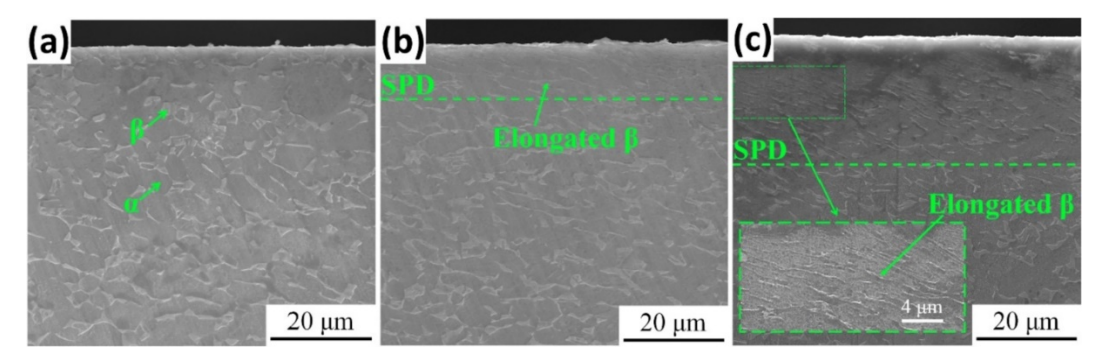


Fig. 25. Cross-sectional SEM images of untreated (a), UNSM (b), and LA-UNSM (c) processed Ti64 alloys [24]. (Used with permission.)

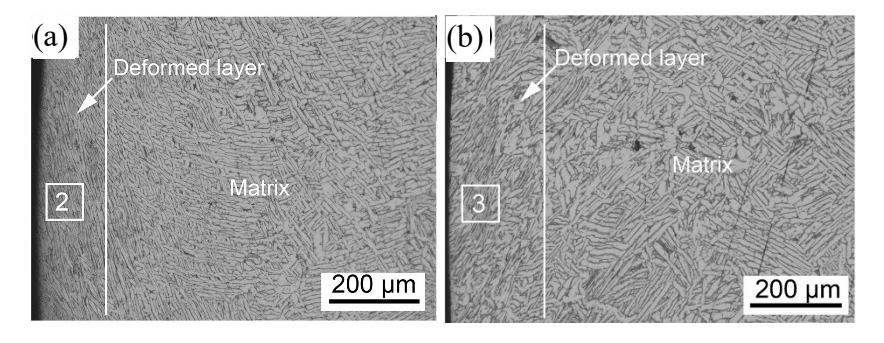


Fig. 26. Microstructures of (a) USRP and (d) DC-USRP processed Ti64 alloy [63]. (Used with permission.)

## 4.2.3. Friction and wear behaviors

Most of the thermally assisted UNSM and USRP works to date reported that the higher working temperature can help to decrease the friction coefficient of the processed workpieces. Wang et al. found that the friction coefficient of the DC-USRP processed Ti64 alloy was slightly lower than the conventional USRP processed one [63]. As shown in Fig. 27a, both USRP and DC-USRP can significantly decrease the friction coefficient of the as-built AM Ti64 alloy. The friction coefficients of the USRP and DC-USRP processed workpieces were 0.15 and 0.14, respectively. Amanov et al. carried out friction tests on Ti64, IN690, and Ta workpieces processed by conventional and HT UNSM [23][58][59]. For Ti64 alloy and Ta, it was reported that friction coefficients of HT UNSM processed workpieces were decreased as compared with those of the conventional UNSM processed ones. However, for IN690 alloy, friction coefficients from HT UNSM were found to be comparable to but slightly higher than that of conventional UNSM processed workpiece. Li et al. also found that friction coefficients of thermally assisted USPR processed Ti64 workpieces were higher than that of the conventional USRP processed one as shown in Fig. 27b [56].

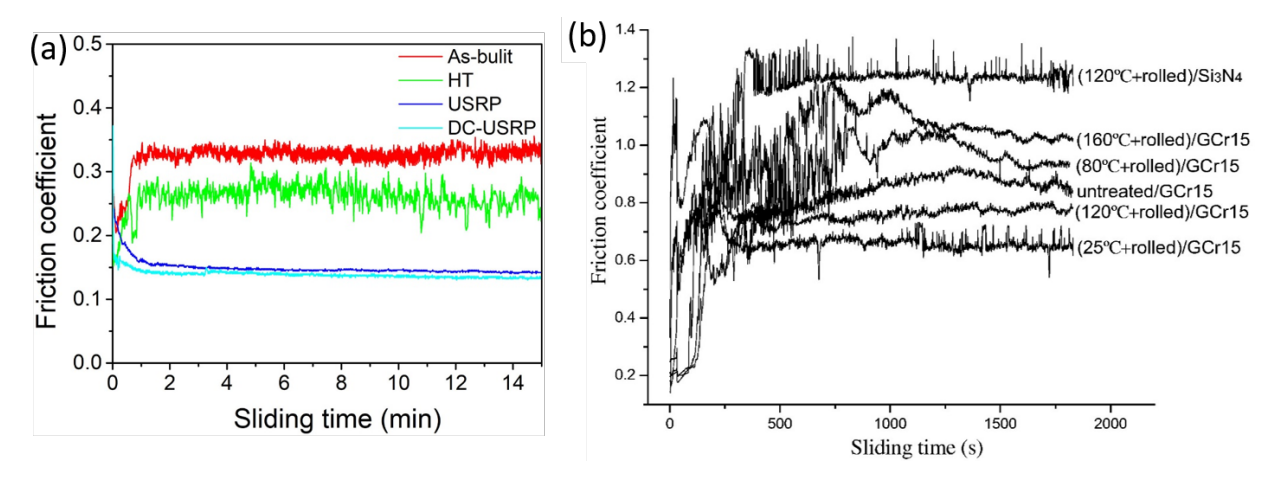


Fig. 27. (a) Friction coefficient as a function of sliding time for (a) AM Ti64 [63] and (b) HIP Ti64 [56] workpieces processed using different conditions. (Used with permission.)

The decrease in friction coefficient can be directly related to the reduced surface roughness [23]. As discussed in Section 4.2.1, thermally assisted USRP and UNSM can produce smoother surfaces in comparison of their conventional counterparts. Additionally, the higher CRS and hardness also contribute to the reduction of the friction coefficient. Studies showed that thermally assisted USRP and UNSM imparted higher and deeper CRS as compared with their conventional counterparts [23][59][60][64]. For example, as show in Fig. 28a, CRS of the conventional UNSM processed Ta workpieces were about -600 MPa in both perpendicular and orthogonal directions, while those of the HT UNSM processed workpiece were -1200 and -1375 MPa, respectively [59]. As shown in Fig. 28b, the USRP performed at high temperatures can increase the CRS depths to a value between 0.5 and 0.6 mm, while that of the conventional USRP processed workpiece was about 0.4 mm. The increased CRS can inhibit crack initiation and thus hider the fracture process, maintaining a smoother surface, which decreases the friction coefficient.

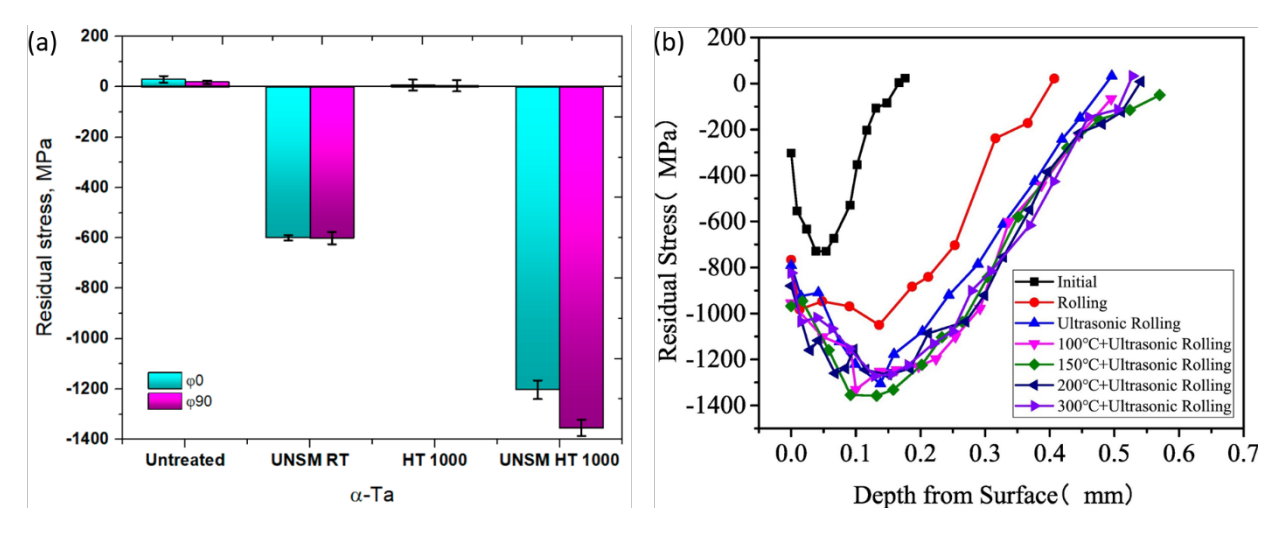


Fig. 28. (a) Surface RS of Ta after different processes [59]. (b) RS distributions of 45CrNiMoVA ultra-high-strength steel after different processes [64]. (Used with permission.)

Metals processed after thermally assisted UNSM or USRP generally have higher wear resistances in comparison of conventional UNSM or USRP processed ones. A comparison between USRP and DC-USRP processed Ti64 alloy in terms of cross-sectional wear track profiles is shown in Fig. 29a [63]. The track width and depth of the DC-USRP processed workpiece were 0.8 mm and 12 μm, while those of the conventional USRP processed workpiece were 0.5 mm and 7 μm, respectively. Improved wear resistances were also reported for Ti64, IN690, and Ta after HT UNSM process [23][58][59]. For example, as shown in Fig. 29b, HT UNSM performed at 1000 °C significantly decrease the wear rate of the Ta workpiece as compared with conventional UNSM [59]. The increased wear resistance can be attributed to the higher CRS and its deeper distribution. Additionally, the thicker hardening layer with higher surface and subsurface strength produced by thermally assisted USRP and UNSM can prevent the surface from being removed, which increases the wear resistance significantly.

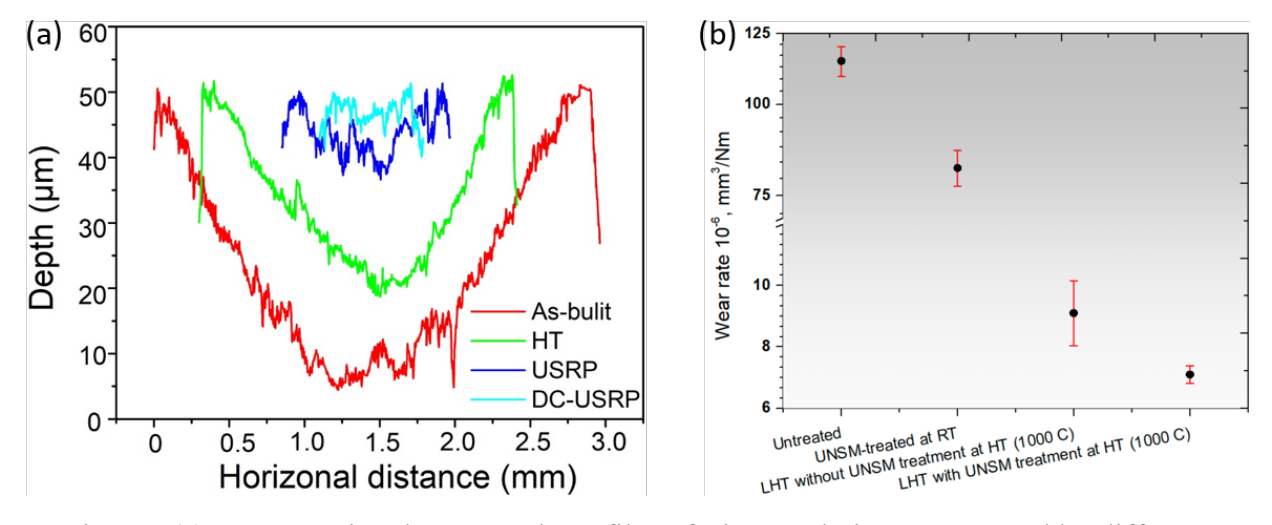


Fig. 29. (a) Cross-sectional wear track profiles of Ti64 workpieces processed by different processes [63]. (b) Wear rates of Ta workpieces processed by different treatments [59]. (Used with permission.)

Table 3. History, cited articles, processed materials, heat sources, working temperatures, and improved mechanical properties of thermally assisted ultrasonic surface hardening, including USRP and UNSM. The effectiveness is quantified by the mechanical property improvement (in %) resulted from the thermally assisted ultrasonic surface hardening performed at the optimal

temperature in comparison of the conventional ultrasonic surface hardening.

emperature in comparison of the conventional uttrasonic surface hardening.						
Year	Material	Heat source	Temperature	Improved mechanical properties		
2017 [56]	Ti64	Copper sleeve wrapped by heating wire	RT, 80, 120, and 160 °C	N/A		
2017 [57]	Ti64	Halogen lamp	RT, 400, 600, and 800 °C	Hardness (146%)		
2017 [23]	Ti64	Halogen lamp	RT, 400, 600, and 800 °C	Hardness (146%) & wear resistance		
2017 [58]	Та	Halogen lamp	RT, 200, and 800 °C	Hardness (185.7%) & wear resistance (50.4%).		
2018 [22]	Ti64	Continuous direct current	RT, 320~550 °C	Hardness (10.2%)		
2018 [62]	AM Ti64	Continuous direct current	RT and 425 °C	Hardness (10.7%)		
2018 [60]	IN690	Halogen lamp	RT, 300, and 700 °C	Hardness (23.9%) & wear resistance		
2018 [59]	Ta	Halogen lamp	RT and 1000 °C	Hardness (155.9%) & wear resistance (60.0%)		
2019 [24]	Ti64	Laser	RT and < 453.5 °C	Hardness (22.2%)		
2020 [63]	AM Ti64	Continuous direct current	RT and 300 °C	Hardness (9.0%) & wear resistance (80%).		
2020 [64]	45CrNiMoVA	Heat circulated oven	RT, 100~300 °C	NA		
2020 [65]	Fe-15Mn-1.2Al- 0.6C high-Mn steel	NA	RT and 300 °C	Suppressed hydrogen infiltration		
2020 [61]	AM 316L	Halogen lamp	RT and 400 °C	Hardness (20%) & wear resistance (10%)		

#### 5. Discussion

With the review of the developments and improved mechanical properties of WSP, WLSP, and thermally assisted ultrasonic surface hardening, it is of specific importance to investigate the fundamental processing mechanisms and to compare the effectiveness of the technologies.

From Table 1, it can be concluded that WSP further enhances the hardness and fatigue life/resistance of carbon steels and aluminum alloys as compared with conventional SP. Wick et al. attributed the enhanced fatigue life/resistance to the higher magnitude and stability of the CRS produced via WSP [25]. The authors claimed that DSA occurred during WSP, producing clouds of carbon atoms and finest carbides, which can anchor the dislocation motion

significantly. For a typical WSP processing, dislocations are produced in the surface and subsurface regions via high-strain-rate plastic deformation. With higher diffusivity promoted at elevated temperature, solute atoms move into the dislocation cores and pin the dislocations. The pinned dislocations interact with the subsequent dislocations produced by the repeated shot peening, increasing the density and stability of dislocations. Such microstructure can enhance the surface hardness of the WSP processed workpiece as compared with conventional SP. Meanwhile, the stable dislocation distribution can also increase the stability of the microscale CRS of the processed workpiece. Therefore, the CRS relaxation of the WSP processed workpiece can be reduced during cyclic loading, leading to enhanced fatigue life/resistance.

WLSP can also increase the hardness and fatigue life/resistance of carbon steels, aluminum alloys, and titanium alloys as compared with conventional LSP. Ye and Liao also attributed the enhancements to the increased stabilities of the CRS and dislocation distribution [21][39]. The DSA effect was proved by the unique dislocation structure induced by WLSP. For example, the authors presented the dislocation structures of the LSP and WLSP processed 4140 steel [21]. As shown in Fig. 30a and 30b, conventional LSP processed 4140 steel demonstrated multiple shear bands and lamellar dislocation boundaries, which were resulted from high-strain-rate plastic deformation. After WLSP, tangled dislocations were produced as shown in Fig. 30c and 30d. Such tangled dislocations were associated with DSA effect. During WLSP, solute atoms can diffuse into the dislocation cores and stay, impeding the dislocation motion. It is thus required higher stress to break the dislocations away. Meanwhile, the high stress produced new dislocations, increasing the dislocation density and enhancing the dislocation multiplication. Therefore, more tangled dislocations were generated after WLSP.

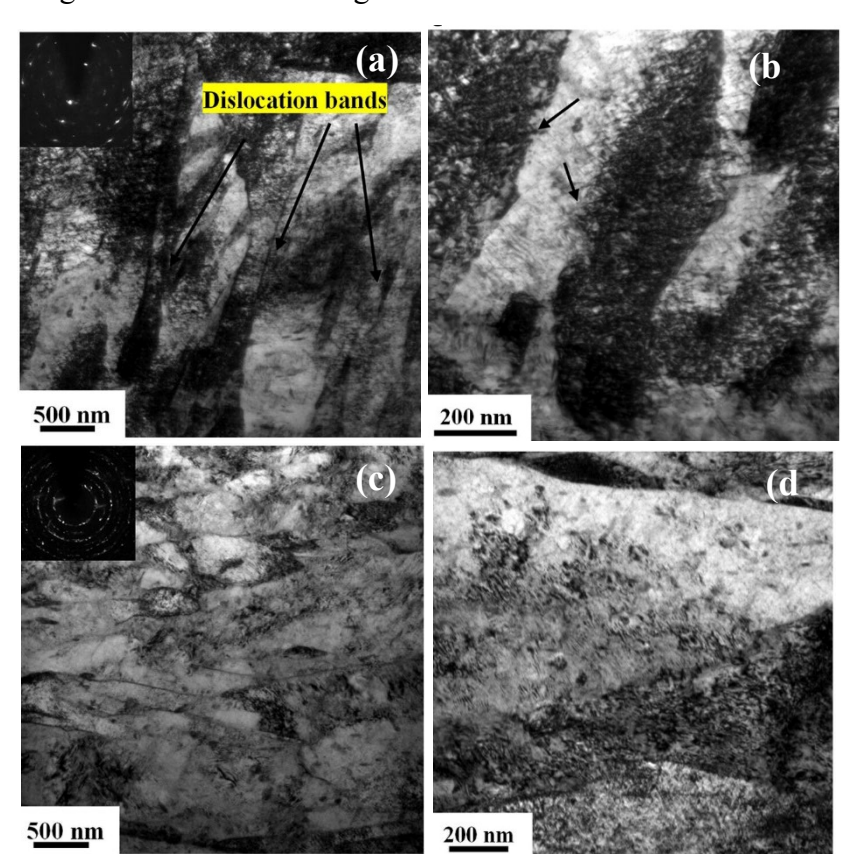


Fig. 30. TEM images of the 4140 steel microstructures after different processes. (a) and (b) Lamellar dislocation bands produced using conventional LSP; (c) and (d) Tangled dislocations produced using WLSP. (Used with permission)

In addition to the DSA effect, it is claimed that nanoscale precipitates can be produced during WLSP via DP and such precipitates can increase the dislocation density and stabilize the microstructure by dislocation pinning. With the help of high-resolution transmission electron microscopy (TEM), the resultant precipitates can be directly observed as shown in Fig. 31. Liao et al. proposed a nucleation model to investigate the DP mechanism during WLSP [39]. It was reported that dislocations produced via peening were the favored nucleation sites for precipitation. DSA can increase the dislocation density via dislocation peening, which further provided nucleation sites for precipitation. Meanwhile, the dislocation core energy can be spent for the nucleation, which decreased the activation energy for precipitation during WLSP. Unlike static aging and static precipitation, the processing time of WLSP is comparatively short and thus the precipitates produced through DP are small since they do not have enough time to grow up. However, such nanoscale precipitates can effectively impede dislocation motion and increase the material strength and the stability of the CRS.

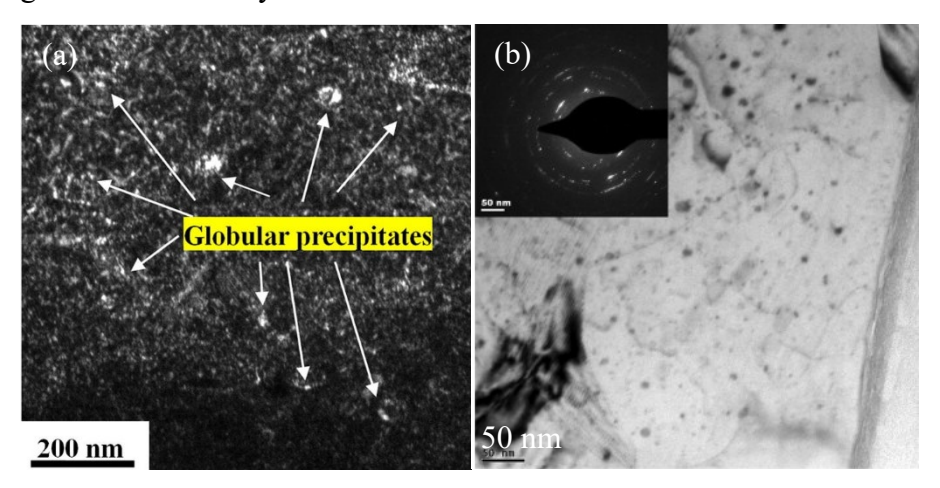


Fig. 31. (a) Dark field TEM image of the AISI 4140 steel processed using WLSP showing the globular nanoprecipitates [21]. (b) TEM image of the AA6061 after WLSP at 160 °C showing the nanoscale precipitates [39]. (Used with permission)

Different from WSP and WLSP, most of the thermally assisted ultrasonic surface hardening studies focus on processing titanium alloys as listed in Table 3. This is because titanium alloys become widely applied in aerospace, chemical, petrochemical, and marine industries due to their excellent properties of high specific strength and corrosion resistance. However, the alloys suffer from low adhesive and fretting wear resistance [66]. Thermally assisted ultrasonic surface hardening therefore has been primarily focus on improving the surface hardness and wear resistance of titanium alloys. Conventional ultrasonic surface hardening can realize severe plastic deformation in the surface or subsurface regions of a metal component, realizing grain refinement and/or nanocrystallization. The refined grains provide higher volume fraction of grain boundaries, which can increase the hardness and wear resistance by impeding dislocation motion. Titanium alloys are typical hard-to-deform materials. They have high work hardening tendency, which makes it challenging to improve the surface strength using conventional ultrasonic surface hardening technique. Additionally, the hexagonal close packed crystal structure of α-Ti poses a

high resistance to plastic deformation because of the limited slip systems and suppression of cross-slip. Ultrasonic surface hardening performed at the optimal temperature can further increase the grain refinement efficiency. Wang et al. reported that USRP performed at RT produced high-density dislocations and refined grains in the surface region of the Ti64 alloy as shown in Fig. 32a [63]. The averaged grain size refined by DC-USRP was about 65 nm as shown in Fig. 32b, which was much smaller than the averaged grain size of 200 nm refined by conventional USRP. With the assistant of the thermal energy, ultrasonic surface hardening can produce more dislocations, enhancing dislocation accumulation and rearrangement [56]. Then, the resultant dislocation structures can subdivide and divide the coarse grains more effectively. Therefore, thermally assisted ultrasonic surface hardening can further increase hardness and wear resistance as compared with its conventional counterpart.

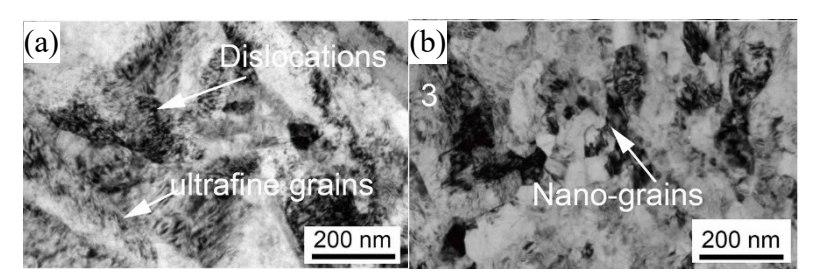


Fig. 32. TEM of the (a) conventional USRP and (b) DC-USRP processed Ti64 workpieces. (Used with permission)

#### 6. Conclusions and outlooks

The present paper reviews the progress and advances of thermally assisted surface hardening for improving mechanical properties of metal components. The process designs of common thermally assisted surface hardening techniques, including WSP, WLSP, and thermally assisted ultrasonic surface strengthening, are introduced. The following conclusion can be drawn:

- Thermally assisted surface hardening performed with optimum processing parameters, can further increase the surface and subsurface hardness, thickness of the hardening layer, fatigue resistance, and/or wear resistance in comparison of conventional surface hardening.
- DSA occurs during WSP, increasing the density and stability of dislocations by pinning the dislocations with solute atoms. Such microstructure can increase the magnitude and stability of the CRS, which increases the fatigue life/resistance of the processed component.
- In addition to DSA, DP can occur during WLSP, leading to high density nanoscale precipitates, which also increase the density and stability of the CRS via impeding dislocation motion.
- Thermally assisted ultrasonic surface strengthening has been mainly applied to process titanium alloys. The thermal energy temporarily decreases the flow stress and facilitates dislocation generation, accumulation, and interaction during processing, resulting in stronger grain refinement effect and increasing the wear resistance.

According to the review above, we try to propose the following future works on thermally assisted surface hardening technology.

### 6.1. Fatigue of thermally assisted ultrasonic surface hardening processed component

As discussed above, WSP and WLSP have been widely applied to improve the fatigue life/resistance of mechanical components. Thermally assisted ultrasonic surface hardening only focus on improving the wear resistance. Therefore, the study on the fatigue life/resistance of thermally assisted ultrasonic surface hardening processed components is expected.

#### 6.2. Corrosion

Corrosion is a primary surface related property for components serving within specific environments. Conventional surface hardening can increase the corrosion resistance through generating a passive film on the surface, acting as a barrier to the subsequent corrosion [67][68][69][70]. The effect of thermally assisted surface hardening on the corrosion behavior of metal components has never been studied. The kinetics of oxidation and nitriding can be increased by the nanostructured surface of a workpiece processed by conventional surface hardening [71][72]. Thermally assisted ultrasonic surface strengthening combines nanocrystallization and elevated temperature annealing together, and it is rational to expect that such synergy could help to produce a thicker passive film in comparison of conventional ultrasonic surface hardening process. Therefore, investigation of the corrosion resistance of components processed by thermally assisted ultrasonic surface hardening might be of great interest to marine industry.

# 6.3. Parameters optimization and computational methods

Thermally assisted surface hardening is a complex post-processing technique because the heat source introduces more processing parameters, including the processing temperature and temperature distributions. The laser beam has great potential to be applied in industries due to the high flexibility of the device. However, the optimization of the laser-assisted surface hardening design is still challenging due to the non-uniform temperature distribution produced by the laser beam. Finding the optimum combination of the heating and surface hardening parameters therefore require a good understanding of the process physics. Computational or numerical modeling, such as finite element analysis (FEA), might be able to provide such understanding as a good substitute to the expensive experimental studies. It was presented that FEA was capable of predicting the gradient temperature distribution induced by the laser beam [73] and residual stress induced by surface hardening [74]. Further work should focus on modeling the synergy of the thermomechanical processing.

# 6.4. Application of thermally assisted surface hardening to ceramic and AM metals

Most of the thermally assisted surface hardening studies have been focused on metallic materials, while no research has been conducted on ceramics. Processing of ceramics using surface hardening techniques has been thought to be impossible since the materials can be broken with little elastic deformation or without significant plastic deformation. However, Pfeiffer and Frey studied the effects of conventional SP on alumina and silicon nitride ceramics [75]. They found that SP can produce microplastic deformation and CRS up to 2 GPa in the surface regions of ceramics. Shukla et al. reported LSP of alumina ceramic [76]. After LSP, the surface hardness of the ceramic was increased by 10%, fracture toughness was increased by 12%, and averaged RS of -64 MPa was produced while that of the untreated ceramic was 219 MPa. In these works, processing parameters such as peening pressure and laser intensity, had to be selected cautiously to avoid brittle failure of the surface. Thermally assisted surface hardening is expected to reduce

the brittleness of the materials via annealing, allowing surface hardening to introduce more plastic deformation and CRS.

Additive manufacturing is attracting increasing attention in a broad range of industries. However, due to the complex thermal histories of different discrete volumes, AM components suffer from material discontinuities, including gas pores and coarse grains [77]. These microstructures reduce mechanical properties such as fracture toughness and fatigue life as well as poor surface finish. To date, only a limited number of related studies were presented, which focus on effects of thermally assisted surface hardening on AM Ti64 and stainless steel 316L [61][62][63]. Therefore, more studies on different AM metals are required in order to spread the technique for industrial applications.

# 6.5. Integration of thermally assisted surface hardening in additive manufacturing

The integration of the surface hardening process with an additive manufacturing process can benefit the mechanical component quality by efficiently modify the microstructure. AM employs a moving heat source to sinter or melt metal powders layer-by-layer. The moving heat source produces a heat-affected zone (HAZ) with solidified region being exposed to elevated temperatures. The surface hardening can be employed to process the HAZ during additive manufacturing processing, realizing thermally assisted surface hardening. The integration should be in such a way that the movement of the surface hardening tool can be controlled in accordance with the heat source in relation to the component position. Therefore, future work should focus on development of integrated surface hardening - AM systems.

## Acknowledgements

This work was supported in part by the Manufacturing Machines & Equipment program of the National Science Foundation under award number 1762678.

### Nomenclature

SP – shot peening

SMAT – surface mechanical attrition

LSP – laser shock peening

CRS – compressive residual stress

UIT – ultrasonic impact treatment

USRP – ultrasonic surface rolling processing

UNSM – ultrasonic nanocrystal surface modification

WSP – warm shot peening

WLSP – warm laser shock peening

RT – room temperature

Ra – arithmetical mean roughness

Ti – titanium

DSA – dynamic strain aging

BCC – body-centered cubic

FCC – face-centered cubic

DP – dynamic precipitation

WLSPwC – warm laser shock peening without coating

CW – continuous wave

IN – Inconel

TZM – titanium-zirconium-molybdenum

SAE – Society of Automotive Engineers

HIP – hot isostatic pressing

HT – high temperature

LA-UNSM – laser-assisted ultrasonic nanocrystal surface modification

AM – additive manufactured

SEM – scanning electron microscopy

TEM – transmission electron microscopy

TMT – thermomechanical treatment

FEA – finite element analysis

UTS – ultimate tensile strength

YS – yield strength

#### References

- [1] M.A.S. Torres, H.J.C. Voorwald, An evaluation of shot peening, residual stress and stress relaxation on the fatigue life of AISI 4340 steel, Int. J. Fatigue. 24 (2002) 877–886. https://doi.org/10.1016/S0142-1123(01)00205-5.
- [2] K. Lu, J. Lu, Nanostructured surface layer on metallic materials induced by surface mechanical attrition treatment, Mater. Sci. Eng. A. 375–377 (2004) 38–45. https://doi.org/10.1016/j.msea.2003.10.261.
- [3] J. Gu, X. Wu, H. Cuypers, J. Wastiels, Laser shock processing of low carbon steel, WIT Trans. Eng. Sci. 2 (1998) 14. https://doi.org/10.2495/SURF930161.
- [4] J.M. Yang, Y.C. Her, N. Han, A. Clauer, Laser shock peening on fatigue behavior of 2024-T3 Al alloy with fastener holes and stopholes, Mater. Sci. Eng. A. 298 (2001) 296–299. https://doi.org/10.1016/S0921-5093(00)01277-6.
- [5] W. Ting, W. Dongpo, L. Gang, G. Baoming, S. Ningxia, Investigations on the nanocrystallization of 40Cr using ultrasonic surface rolling processing, Appl. Surf. Sci. 255 (2008) 1824–1829. https://doi.org/10.1016/j.apsusc.2008.06.034.
- [6] C. Ye, A. Telang, A.S. Gill, S. Suslov, Y. Idell, K. Zweiacker, J.M.K. Wiezorek, Z. Zhou, D. Qian, S.R. Mannava, V.K. Vasudevan, Gradient nanostructure and residual stresses induced by Ultrasonic Nano-crystal Surface Modification in 304 austenitic stainless steel for high strength and high ductility, Mater. Sci. Eng. A. 613 (2014) 274–288. https://doi.org/10.1016/j.msea.2014.06.114.
- [7] Q. Liu, C.H. Yang, K. Ding, S.A. Barter, L. Ye, The effect of laser power density on the fatigue life of laser-shock-peened 7050 aluminium alloy, Fatigue Fract. Eng. Mater. Struct. 30 (2007) 1110–1124. https://doi.org/10.1111/j.1460-2695.2007.01180.x.
- [8] O. Unal, R. Varol, Almen intensity effect on microstructure and mechanical properties of low carbon steel subjected to severe shot peening, Appl. Surf. Sci. 290 (2014) 40–47. https://doi.org/10.1016/j.apsusc.2013.10.184.
- [9] Y. Liu, D. Wang, C. Deng, L. Xia, L. Huo, L. Wang, B. Gong, Influence of re-ultrasonic impact treatment on fatigue behaviors of S690QL welded joints, Int. J. Fatigue. 66 (2014) 155–160. https://doi.org/10.1016/j.ijfatigue.2014.03.024.
- [10] Y. Feng, S. Hu, D. Wang, L. Cui, Formation of short crack and its effect on fatigue properties of ultrasonic peening treatment S355 steel, Mater. Des. 89 (2016) 507–515. https://doi.org/10.1016/j.matdes.2015.10.009.
- [11] S.D. Mesarovic, Dynamic strain aging and plastic instabilities, J. Mech. Phys. Solids. 43 (1995) 671–700. https://doi.org/10.1016/0022-5096(95)00010-G.
- [12] A.H. Cottrell, B.A. Bilby, Dislocation Theory of Yielding and Strain Ageing of Iron, Proc. Phys. Soc. Sect. A. 62 (1949) 49–62. https://doi.org/10.1088/0370-1298/62/1/308.

- [13] R.A. Mulford, U.F. Kocks, New observations on the mechanisms of dynamic strain aging and of jerky flow, Acta Metall. 27 (1979) 1125–1134. https://doi.org/10.1016/0001-6160(79)90130-5.
- [14] J.G. Morris, Dynamic strain aging in aluminum alloys, Mater. Sci. Eng. 13 (1974) 101–108. https://doi.org/10.1016/0025-5416(74)90177-3.
- [15] D. Blavette, Three-Dimensional Atomic-Scale Imaging of Impurity Segregation to Line Defects, Science (80-.). 286 (1999) 2317–2319. https://doi.org/10.1126/science.286.5448.2317.
- [16] O. Waseda, R.G. Veiga, J. Morthomas, P. Chantrenne, C.S. Becquart, F. Ribeiro, A. Jelea, H. Goldenstein, M. Perez, Formation of carbon Cottrell atmospheres and their effect on the stress field around an edge dislocation, Scr. Mater. 129 (2017) 16–19. https://doi.org/10.1016/j.scriptamat.2016.09.032.
- [17] E. Kerscher, K.H. Lang, O. Vöhringer, D. Löhe, Increasing the fatigue limit of a bearing steel by dynamic strain ageing, Int. J. Fatigue. 30 (2008) 1838–1842. https://doi.org/10.1016/j.ijfatigue.2008.02.003.
- [18] M. Cai, D.P. Field, G.W. Lorimer, A systematic comparison of static and dynamic ageing of two Al-Mg-Si alloys, Mater. Sci. Eng. A. 373 (2004) 65–71. https://doi.org/10.1016/j.msea.2003.12.035.
- [19] A. Tange, H. Koyama, H. Tsuji, J. Schaad, Study on Warm Shot Peening for Suspension Coil Spring, J. Mater. Manuf. 108 (1999) 463–467. https://doi.org/10.4271/1999-01-0415.
- [20] A. Wick, V. Schulze, O. Vöhringer, Effects of warm peening on fatigue life and relaxation behaviour of residual stresses in AISI 4140 steel, Mater. Sci. Eng. A. 293 (2000) 191–197. https://doi.org/10.1016/S0921-5093(00)01035-2.
- [21] C. Ye, S. Suslov, B.J. Kim, E.A. Stach, G.J. Cheng, Fatigue performance improvement in AISI 4140 steel by dynamic strain aging and dynamic precipitation during warm laser shock peening, Acta Mater. 59 (2011) 1014–1025. https://doi.org/10.1016/j.actamat.2010.10.032.
- [22] J. Liu, S. Suslov, S. Li, H. Qin, Z. Ren, G.L. Doll, H. Cong, Y. Dong, C. Ye, Electrically Assisted Ultrasonic Nanocrystal Surface Modification of Ti6Al4V Alloy, Adv. Eng. Mater. 20 (2018) 1–6. https://doi.org/10.1002/adem.201700470.
- [23] A. Amanov, Y.S. Pyun, Local heat treatment with and without ultrasonic nanocrystal surface modification of Ti-6Al-4V alloy: Mechanical and tribological properties, Surf. Coatings Technol. 326 (2017) 343–354. https://doi.org/10.1016/j.surfcoat.2017.07.064.
- [24] J. Liu, S. Suslov, Z. Ren, Y. Dong, C. Ye, Microstructure evolution in Ti64 subjected to laser-assisted ultrasonic nanocrystal surface modification, Int. J. Mach. Tools Manuf. 136 (2019) 19–33. https://doi.org/10.1016/j.ijmachtools.2018.09.005.
- [25] A. Wick, V. Schulze, O. Vohringer, Influence of the shot peening temperature on the relaxation behaviour of residual stresses during cyclic bending, in: 7th Int. Conf. SHOT Peen., Warsaw, Poland, 1999: pp. 102–109.

- [26] R. Menig, V. Schulze, O. Vöhringer, Optimized warm peening of the quenched and tempered steel AISI 4140, Mater. Sci. Eng. A. 335 (2002) 198–206. https://doi.org/10.1016/S0921-5093(01)01915-3.
- [27] W. Luan, C. Jiang, V. Ji, Y. Chen, H. Wang, Investigation for warm peening of TiB2/Al composite using X-ray diffraction, Mater. Sci. Eng. A. 497 (2008) 374–377. https://doi.org/10.1016/j.msea.2008.07.016.
- [28] W. Luan, C. Jiang, V. Ji, The texture effect of warm peening on TiB2/Al composite, Mater. Sci. Eng. A. 504 (2009) 124–128. https://doi.org/10.1016/j.msea.2008.10.035.
- [29] M. Thomas, M. Jackson, The role of temperature and alloy chemistry on subsurface deformation mechanisms during shot peening of titanium alloys, Scr. Mater. 66 (2012) 1065–1068. https://doi.org/10.1016/j.scriptamat.2012.02.049.
- [30] J. Huang, Z. Wang, K. Bian, C. Jiang, Investigation for different peening techniques on residual stress field of SiCw/Al composite, J. Mater. Eng. Perform. 22 (2013) 782–786. https://doi.org/10.1007/s11665-012-0303-3.
- [31] J. Huang, Z. Wang, J. Gan, Y. Yang, G. Wu, Q. Meng, Investigation of fatigue performance improvement in SiCw/Al composites with different modified shot peening treatments by considering surface mechanical properties, J. Alloys Compd. 728 (2017) 169–178. https://doi.org/10.1016/j.jallcom.2017.08.269.
- [32] Y. Huang, W.C. Liu, J. Dong, Surface characteristics and fatigue performance of warm shot peened wrought magnesium alloy Mg-9Gd-2Y, Mater. Sci. Technol. (United Kingdom). 30 (2014) 1481–1487. https://doi.org/10.1179/1743284713Y.0000000450.
- [33] Y. Harada, K. Mori, Effect of processing temperature on warm shot peening of spring steel, J. Mater. Process. Technol. 162–163 (2005) 498–503. https://doi.org/10.1016/j.jmatprotec.2005.02.095.
- [34] Y. Harada, K. Fukauara, S. Kohamada, Effects of microshot peening on surface characteristics of high-speed tool steel, J. Mater. Process. Technol. 201 (2008) 319–324. https://doi.org/10.1016/j.jmatprotec.2007.11.247.
- [35] A. Tange, K. Ando, Improvement of spring fatigue strength by new warm stress double shot peening process, Mater. Sci. Technol. 18 (2002) 642–648. https://doi.org/10.1179/026708302225003514.
- [36] Y. Harada, K. Fukaura, S. Haga, Influence of microshot peening on surface layer characteristics of structural steel, J. Mater. Process. Technol. 191 (2007) 297–301. https://doi.org/10.1016/j.jmatprotec.2007.03.026.
- [37] C. Ye, Y. Liao, G.J. Cheng, Warm laser shock peening driven nanostructures and their effects on fatigue performance in Aluminum Alloy 6160, Adv. Eng. Mater. 12 (2010) 291–297. https://doi.org/10.1002/adem.200900290.
- [38] C. Ye, G.J. Cheng, Effects of Temperature on Laser Shock Induced Plastic Deformation: The Case of Copper, J. Manuf. Sci. Eng. 132 (2010) 61009. https://doi.org/10.1115/1.4002849.

- [39] Y. Liao, C. Ye, B.J. Kim, S. Suslov, E.A. Stach, G.J. Cheng, Nucleation of highly dense nanoscale precipitates based on warm laser shock peening, J. Appl. Phys. 108 (2010). https://doi.org/10.1063/1.3481858.
- [40] G. Tani, L. Orazi, A. Fortunato, A. Ascari, G. Campana, Warm Laser Shock Peening: New developments and process optimization, CIRP Ann. Manuf. Technol. 60 (2011) 219–222. https://doi.org/10.1016/j.cirp.2011.03.115.
- [41] J.Z. Zhou, X.K. Meng, S. Huang, J. Sheng, J.Z. Lu, Z.R. Yang, C. Su, Effects of warm laser peening at elevated temperature on the low-cycle fatigue behavior of Ti6Al4V alloy, Mater. Sci. Eng. A. 643 (2015) 86–95. https://doi.org/10.1016/j.msea.2015.07.017.
- [42] Y. Liao, C. Ye, G.J. Cheng, [INVITED] A review: Warm laser shock peening and related laser processing technique, Opt. Laser Technol. 78 (2016) 15–24. https://doi.org/10.1016/j.optlastec.2015.09.014.
- [43] S. Prabhakaran, S. Kalainathan, Warm laser shock peening without coating induced phase transformations and pinning effect on fatigue life of low-alloy steel, Mater. Des. 107 (2016) 98–107. https://doi.org/10.1016/j.matdes.2016.06.026.
- [44] H. Chen, J. Zhou, J. Sheng, X. Meng, S. Huang, X. Xie, Effects of warm laser Peening on thermal stability and high temperature mechanical properties of A356 Alloy, Metals (Basel). 6 (2016). https://doi.org/10.3390/met6060126.
- [45] X. Meng, J. Zhou, C. Su, S. Huang, K. Luo, J. Sheng, W. Tan, Residual stress relaxation and its effects on the fatigue properties of Ti6Al4V alloy strengthened by warm laser peening, Mater. Sci. Eng. A. 680 (2017) 297–304. https://doi.org/10.1016/j.msea.2016.10.073.
- [46] X. Meng, Y. Zhao, J. Lu, S. Huang, J. Zhou, C. Su, Improvement of damping property and its effects on the vibration fatigue in Ti6Al4V titanium alloy treated by warm laser shock peening, Metals (Basel). 9 (2019). https://doi.org/10.3390/met9070746.
- [47] J.Z.Z. Lu, H.F.F. Duan, K.Y.Y. Luo, L.J.J. Wu, W.W.W. Deng, J. Cai, Tensile properties and surface nanocrystallization analyses of H62 brass subjected to room-temperature and warm laser shock peening, J. Alloys Compd. 698 (2017) 633–642. https://doi.org/10.1016/j.jallcom.2016.12.210.
- [48] J. Sheng, S. Huang, J.Z. Zhou, Z.W. Wang, Effects of warm laser peening on the elevated temperature tensile properties and fracture behavior of IN718 nickel-based superalloy, Eng. Fract. Mech. 169 (2017) 99–108. https://doi.org/10.1016/j.engfracmech.2016.11.016.
- [49] T. Hu, S. Li, H. Qiao, Y. Lu, B. Sun, J. Wu, Effect of Warm Laser Shock Peening on Microstructure and Properties of GH4169 Superalloy, in: IOP Conf. Ser. Mater. Sci. Eng., 2018. https://doi.org/10.1088/1757-899X/423/1/012054.
- [50] Y. Lu, J. Zhao, H. Qiao, T. Hu, B. Sun, J. Wu, A study on the surface morphology evolution of the GH4619 using warm laser shock peening, AIP Adv. 9 (2019). https://doi.org/10.1063/1.5082755.
- [51] C. Duan, X. Hao, Y. Pei, X. Luo, Stress Wave and Residual Stress Characteristics of TC17 Titanium Alloy Subjected to Warm Laser Shock Peening, Adv. Eng. Mater. 21

- (2019) 1–10. https://doi.org/10.1002/adem.201800448.
- [52] G. V. Inamke, L. Pellone, J. Ning, Y.C. Shin, Enhancement of weld strength of laser-welded joints of AA6061-T6 and TZM alloys via novel dual-laser warm laser shock peening, Int. J. Adv. Manuf. Technol. 104 (2019) 907–919. https://doi.org/10.1007/s00170-019-03868-y.
- [53] E.S. Statnikov, O. V. Korolkov, V.N. Vityazev, Physics and mechanism of ultrasonic impact, Ultrasonics. 44 (2006) 533–538. https://doi.org/10.1016/j.ultras.2006.05.119.
- [54] A.T. Bozdana, N.N.Z. Gindy, H. Li, Deep cold rolling with ultrasonic vibrations A new mechanical surface enhancement technique, Int. J. Mach. Tools Manuf. 45 (2005) 713–718. https://doi.org/10.1016/j.ijmachtools.2004.09.017.
- [55] C.M. Suh, G.H. Song, M.S. Suh, Y.S. Pyoun, Fatigue and mechanical characteristics of nano-structured tool steel by ultrasonic cold forging technology, Mater. Sci. Eng. A. 443 (2007) 101–106. https://doi.org/10.1016/j.msea.2006.08.066.
- [56] G. Li, S. Qu, M.X. Xie, X. Li, Effect of ultrasonic surface rolling at low temperatures on surface layer microstructure and properties of HIP Ti-6Al-4V alloy, Surf. Coatings Technol. 316 (2017) 75–84. https://doi.org/10.1016/j.surfcoat.2017.01.099.
- [57] A. Amanov, B. Urmanov, T. Amanov, Y.S. Pyun, Strengthening of Ti-6Al-4V alloy by high temperature ultrasonic nanocrystal surface modification technique, Mater. Lett. 196 (2017) 198–201. https://doi.org/10.1016/j.matlet.2017.03.059.
- [58] A. Amanov, Y.S. Pyun, V.K. Vasudevan, High Strength and Wear Resistance of Tantalum by Ultrasonic Nanocrystalline Surface Modification Technique at High Temperatures, IOP Conf. Ser. Mater. Sci. Eng. 194 (2017). https://doi.org/10.1088/1757-899X/194/1/012032.
- [59] J.M. Chae, K.O. Lee, A. Amanov, Gradient nanostructured tantalum by thermal-mechanical ultrasonic impact energy, Materials (Basel). 11 (2018) 1–18. https://doi.org/10.3390/ma11030452.
- [60] A. Amanov, R. Umarov, The effects of ultrasonic nanocrystal surface modification temperature on the mechanical properties and fretting wear resistance of Inconel 690 alloy, Appl. Surf. Sci. 441 (2018) 515–529. https://doi.org/10.1016/j.apsusc.2018.01.293.
- [61] A. Amanov, Effect of local treatment temperature of ultrasonic nanocrystalline surface modification on tribological behavior and corrosion resistance of stainless steel 316L produced by selective laser melting, Surf. Coatings Technol. 398 (2020) 126080. https://doi.org/10.1016/j.surfcoat.2020.126080.
- [62] H. Zhang, J. Zhao, J. Liu, H. Qin, Z. Ren, G.L. Doll, Y. Dong, C. Ye, The effects of electrically-assisted ultrasonic nanocrystal surface modification on 3D-printed Ti-6Al-4V alloy, Addit. Manuf. 22 (2018) 60–68. https://doi.org/10.1016/j.addma.2018.04.035.
- [63] Z. Wang, Z. Liu, C. Gao, K. Wong, S. Ye, Z. Xiao, Modified wear behavior of selective laser melted Ti6Al4V alloy by direct current assisted ultrasonic surface rolling process, Surf. Coatings Technol. 381 (2020) 125122. https://doi.org/10.1016/j.surfcoat.2019.125122.

- [64] X. Luan, W. Zhao, Z. Liang, S. Xiao, G. Liang, Y. Chen, S. Zou, X. Wang, Experimental study on surface integrity of ultra-high-strength steel by ultrasonic hot rolling surface strengthening, Surf. Coatings Technol. 392 (2020) 125745. https://doi.org/10.1016/j.surfcoat.2020.125745.
- [65] J.G. Kim, H.J. Seo, J.M. Park, S.M. Baek, A. Amanov, C.S. Lee, H.S. Kim, The role of ultrasonic nanocrystalline surface modification at elevated temperature on the hydrogen charging behavior of high-Mn steels, Materialia. 9 (2020) 100626. https://doi.org/10.1016/j.mtla.2020.100626.
- [66] K.G. Budinski, Tribological properties of titanium-alloys, Wear. 151 (1991) 203–217. https://doi.org/10.1016/0043-1648(91)90249-T.
- [67] U. Trdan, J. Grum, Evaluation of corrosion resistance of AA6082-T651 aluminium alloy after laser shock peening by means of cyclic polarisation and ElS methods, Corros. Sci. 59 (2012) 324–333. https://doi.org/10.1016/j.corsci.2012.03.019.
- [68] V. Azar, B. Hashemi, M. Rezaee Yazdi, The effect of shot peening on fatigue and corrosion behavior of 316L stainless steel in Ringer's solution, Surf. Coatings Technol. 204 (2010) 3546–3551. https://doi.org/10.1016/j.surfcoat.2010.04.015.
- [69] H. Lim, P. Kim, H. Jeong, S. Jeong, Enhancement of abrasion and corrosion resistance of duplex stainless steel by laser shock peening, J. Mater. Process. Technol. 212 (2012) 1347–1354. https://doi.org/10.1016/j.jmatprotec.2012.01.023.
- [70] X. Hou, S. Mankoci, N. Walters, H. Gao, R. Zhang, S. Li, H. Qin, Z. Ren, G.L. Doll, H. Cong, A. Martini, V.K. Vasudevan, X. Zhou, N. Sahai, Y. Dong, C. Ye, Hierarchical structures on nickel-titanium fabricated by ultrasonic nanocrystal surface modification, Mater. Sci. Eng. C. 93 (2018) 12–20. https://doi.org/10.1016/j.msec.2018.07.032.
- [71] J. Liu, S. Suslov, S. Li, H. Qin, Z. Ren, C. Ma, G.-X.X. Wang, G.L. Doll, H. Cong, Y. Dong, C. Ye, Effects of ultrasonic nanocrystal surface modification on the thermal oxidation behavior of Ti6Al4V, Surf. Coatings Technol. 325 (2017) 289–298. https://doi.org/10.1016/j.surfcoat.2017.04.051.
- [72] W.P. Tong, Nitriding Iron at Lower Temperatures, Science (80-.). 299 (2003) 686–688. https://doi.org/10.1126/science.1080216.
- [73] J. Yang, S. Sun, M. Brandt, W. Yan, Experimental investigation and 3D finite element prediction of the heat affected zone during laser assisted machining of Ti6Al4V alloy, J. Mater. Process. Technol. 210 (2010) 2215–2222. https://doi.org/10.1016/j.jmatprotec.2010.08.007.
- [74] J. Liu, X. Hou, C. Ye, Y. Dong, Formation mechanism of hierarchical pattern fabricated by ultrasonic-assisted texturing: dynamic indentation induced pile-up, Appl. Surf. Sci. 536 (2021). https://doi.org/10.1016/j.apsusc.2020.147867.
- [75] W. Pfeiffer, T. Frey, Strengthening of ceramics by shot peening, J. Eur. Ceram. Soc. 26 (2006) 2639–2645. https://doi.org/10.1016/j.jeurceramsoc.2005.06.036.
- [76] P. Shukla, S. Robertson, H. Wu, A. Telang, M. Kattoura, S. Nath, S.R. Mannava, V.K. Vasudevan, J. Lawrence, Surface engineering alumina armour ceramics with laser shock

- peening, Mater. Des. 134 (2017) 523-538. https://doi.org/10.1016/j.matdes.2017.08.066.
- [77] P.C. Collins, D.A. Brice, P. Samimi, I. Ghamarian, H.L. Fraser, Microstructural Control of Additively Manufactured Metallic Materials, Annu. Rev. Mater. Res. 46 (2016) 63–91. https://doi.org/10.1146/annurev-matsci-070115-031816.